Local discontinuous Galerkin methods for diffusive-viscous wave equations

Dan Ling[1], Chi-Wang Shu[2], Wenjing Yan[3]

Abstract

Numerical simulation of seismic wave equations has attracted much attention and plays a significant role in exploration seismology. As one of seismic wave models, the diffusive-viscous wave theory usually describes the attenuation of seismic wave propagating in fluid-saturated medium. In this paper, we focus on the design of numerical methods for the diffusive-viscous wave equations with variable coefficients. We develop a local discontinuous Galerkin (LDG) method, in which numerical fluxes are chosen carefully to maintain stability and accuracy. Moreover, we also prove the optimal error estimates for both the energy norm and the L^2 norm. Numerical experiments are provided to demonstrate the optimal convergence rate and effectiveness of the proposed LDG method.

Keywords: Diffusive-viscous wave equations; variable coefficients; local discontinuous Galerkin method; optimal error estimates.

[1]School of Mathematics and Statistics, Xi'an Jiaotong University, Xi'an, Shaanxi 710049, China. E-mail: danling@xjtu.edu.cn. Research partially supported by National Natural Science Foundation of China grant 12101486, China Postdoctoral Science Foundation grant 2020M683446 and the High-performance Computing Platform at Xi'an Jiaotong University.

[2]Division of Applied Mathematics, Brown University, Providence, RI 02912, USA. E-mail: chi-wang_shu@brown.edu. Research partially supported by NSF grant DMS-2010107 and AFOSR grant FA9550-20-1-0055.

[3]School of Mathematics and Statistics, Xi'an Jiaotong University, Xi'an, Shaanxi 710049, China. E-mail: wenjingyan@xjtu.edu.cn. Research partially supported by National Natural Science Foundation of China grant 11971377.

1 Introduction

Numerical modeling of seismic wave equations plays a significant role in exploration seismology and also is an efficient approach to study seismic interpretation and evaluation, and to design seismic survey. Up to now, there have been several types of theoretical models to describe different physical phenomena observed in seismic data, such as Biot's theory [1, 2, 3], squirt-flow mechanism [14], etc.

In seismic exploration, the frequency-dependent reflection occurrences have become an increasingly instrumental part in hydrocarbon exploration and have become more popular [15, 19]. In a reservoir, the relationship between the frequency-dependent reflections and the fluid saturation is relatively complex. From the laboratory analysis and field data, the reflections from a fluid-saturated medium have a higher amplitude and delayed travel-time at low-frequencies when compared with the reflections from a gas-saturated layer. This observed phenomena cannot be described well by Biot's theory [15]. Also, the acoustic and elastic theories are unable to effectively characterize the subsurface in fluid-saturated rocks. In order to simulate wave propagation and make a wider application in practical seismic exploration, Korneev et al. [19] proposed the diffusive-viscous theory, in which they added a diffusive dissipation term and a viscous term to the scalar wave equation. This model can establish the relationship between the frequency dependence of reflections and fluid-saturation in the porous medium. Numerous simulations have shown that the field observations agree with the effects seen in the seismic data and predicted by the diffusive-viscous wave equations. This theory can also be applied to identify oil and gas reservoirs through abstracting the low-frequency shadow phenomenon from seismic data [17].

In the past several years, the study on the diffusive-viscous equations has attracted an increasing interest in the scientific and industrial communities. Quintal et al. [22] used Biot's theory and one-dimensional finite-difference model to study the reflections in the low-frequency range, and proposed the interlayer-flow model, which provides a physical basis to the diffusive-viscous theory, and can explain the spectral anomalies observed at low frequencies in thinly

layered reservoirs. To simulate the frequency-dependent seismic response of turbidite reservoirs, Chen et al. [4] applied a seismic data-driven geological model to produce physical parameter sections and then used it to numerically solve the diffusive-viscous wave equations. Zhao et al. proposed the finite difference method to simulate wave-fields of the diffusive-viscous wave equations in [25, 26], and studied the von Neumann stability criteria and analyzed the numerical dispersion [25]. In a recent paper, Mensah et al. [21] developed a finite volume method to simulate seismic wave propagation in a fluid-saturated medium driven by the diffusive-viscous wave equations. For a general initial-boundary value problem of the diffusive-viscous wave equation, the authors in [16] proved the well-posedness of such a problem, and established a theoretical foundation to develop numerical methods for solving the diffusive-viscous wave equations.

In recent years, the discontinuous Galerkin (DG) method has been widely applied to solve linear and nonlinear time-dependent problems, coupled with the Runge-Kutta time discretization. It was originally proposed to solve hyperbolic conservation laws with only first-order spatial derivatives, e.g. [7, 8, 9, 11, 12]. The DG method has many advantages such as high order accuracy, geometric flexibility, suitability for h- and p-adaptivity, extremely local data structure, high parallel efficiency and a good theoretical foundation for stability and error estimates. It was later generalized to the local DG (LDG) method by Cockburn and Shu to solve the problems with high-order spatial derivatives, such as convection-diffusion equations [10]. After that, the LDG method has been a popular way to solve the problems with second or higher order spatial derivatives, including convection-diffusion equations [5], second order wave equations [6, 23], KdV type equations [24] and fourth order problems [13, 20], etc.

In this paper, we develop an LDG scheme for the one- and two-dimensional diffusive-viscous wave equations with variable coefficients, which is more suitable for studying the relationship between the frequency dependence of reflections and fluid-saturation in a porous medium. To ensure stability, the alternating numerical fluxes are taken and extra attention is paid at the interface when the coefficients are discontinuous. We also prove that the proposed LDG method

has the optimal convergence rates both in the energy and in the L^2 norms. To the best of our knowledge, this is the first time LDG method has been applied to the diffusive-viscous wave equations. From the numerical results, the LDG method can effectively simulate the seismic wave propagation in heterogeneous media, which allows a wider application of this method.

The organization of the paper is as follows. In Section 2, we first introduce some notations and then present the semi-discrete LDG method, and prove the property of energy decay. In Section 3, we analyze the optimal error estimates both in the energy norm and in the L^2 norm. The fully discrete LDG method with the Runge-Kutta method for the time discretization is shown in Section 4. In Section 5, numerical experiments are performed to test the optimal convergence order and effectiveness of the proposed LDG method. Finally, we give some concluding remarks in Section 6.

2 Local discontinuous Galerkin method

2.1 The governing equation

We consider the following diffusive-viscous wave equation:

$$\frac{\partial^2 u}{\partial t^2} + \alpha \frac{\partial u}{\partial t} - \frac{\partial}{\partial t}\mathrm{div}(\beta^2 \nabla u) - \mathrm{div}(\gamma^2 \nabla u) = f, \quad \boldsymbol{x} \in \Omega, \quad t \in [0, T]. \tag{2.1}$$

Here, $u = u(\boldsymbol{x}, t)$ is the wave field, $\alpha = \alpha(\boldsymbol{x}) \geq 0$ and $\beta = \beta(\boldsymbol{x}) \geq 0$ are the diffusive and viscous attenuation parameters respectively, $\gamma = \gamma(\boldsymbol{x}) > 0$ is the wave propagation speed in the non-dispersive medium, $f = f(\boldsymbol{x}, t)$ is the source which generates the vibration. This problem needs to be equipped with following initial conditions

$$u(\boldsymbol{x}, 0) = u_0(\boldsymbol{x}), \quad u_t(\boldsymbol{x}, 0) = v_0(\boldsymbol{x}). \tag{2.2}$$

In this paper, we will assume that $\alpha(\boldsymbol{x}), \beta(\boldsymbol{x}), \gamma(\boldsymbol{x})$ are all piecewise smooth and consider both periodic and homogeneous Dirichlet boundary conditions. Here, we remark that the results in the following will remain the same whether a source term $f(\boldsymbol{x}, t)$ is added or not. Hence, for simplicity, we just consider (2.1) with $f = 0$ throughout the paper.

2.2 Notations

We focus on two dimensions and write $\boldsymbol{x}$ as (x, y). Without loss of generality, we consider a rectangular domain denoted by $\Omega = [a, b] \times [c, d]$. The computational domain Ω is discretized into rectangular cells $K_{ij} = I_i \times J_j$, where $I_i = [x_{i-\frac{1}{2}}, x_{i+\frac{1}{2}}],\ i = 1, 2, \cdots, N$ and $J_j = [y_{j-\frac{1}{2}}, y_{j+\frac{1}{2}}],\ j = 1, 2, \cdots, M$. Triangular meshes can also be used for the LDG method but will not be discussed in this paper. The center of the element is denoted by $(x_i, y_j) = \frac{1}{2}\big(x_{i-\frac{1}{2}} + x_{i+\frac{1}{2}}, y_{j-\frac{1}{2}} + y_{j+\frac{1}{2}}\big)$. We also denote the mesh size as $h_i^x = x_{i+\frac{1}{2}} - x_{i-\frac{1}{2}}, h_j^y = y_{j+\frac{1}{2}} - y_{j-\frac{1}{2}}$ with $h^x = \max\limits_{1\le i\le N} h_i^x, h^y = \max\limits_{1\le j\le M} h_j^y$ and $h = \max(h^x, h^y)$ being the maximal mesh size. ∂K is the boundary of the cell K and $\boldsymbol{n}_K$ is the outward unit normal vector of ∂K. In particular, in the one-dimensional case, the computational domain is denoted by $\Omega = [a, b]$ and the cell $K_i = I_i$ is a subinterval, for which the boundaries are the two end points $x_{i-\frac{1}{2}}$ and $x_{i+\frac{1}{2}}$ corresponding to $\boldsymbol{n}_{I_i} = -1$ and 1 respectively.

Let $\mathcal{T}_h$ be the family of the partitions of Ω parameterized by h. $\mathcal{E}_h$ denotes the set of all edges of cells $K_{ij}, i = 1, 2, \cdots, N; j = 1, 2, \cdots, M$. We define the piecewise polynomial space V_h^k as the space of tensor product of P^k, that is

$$V_h^k = \left\{v : v|_K \in Q^k(K),\ \ \forall K \in \mathcal{T}_h\right\}.$$

In the one-dimensional case, $Q^k(K) = P^k(K)$ which is the space of polynomials of degree at most k on each cell K. This definition can be extended to vector-valued functions

$$W_h^k = \left\{\boldsymbol{w} = (w_1, w_2)^{\mathrm{T}} : w_\ell|_K \in Q^k(K), \ell = 1, 2,\ \ \forall K \in \mathcal{T}_h\right\}.$$

We denote the numerical solution by u_h, which belongs to the finite element space V_h^k. $u_h(x^+_{i+\frac{1}{2}}, y)$ and $u_h(x^-_{i+\frac{1}{2}}, y)$ are the limit values of u_h at the interface $x_{i+\frac{1}{2}}$ from the right cell $K_{i+1,j}$ and from the left cell K_{ij}, respectively. Similarly, we can define $u_h(x, y^+_{j+\frac{1}{2}})$ and $u_h(x, y^-_{j+\frac{1}{2}})$.

2.3 The semi-discrete LDG scheme

In this subsection, we present the semi-discrete LDG method for the governing equation in (2.1) by discretizing the space with the LDG method. Two auxiliary variables $\boldsymbol{p} = (p^1, p^2)$ and $\boldsymbol{q} = (q^1, q^2)$ are introduced to substitute the derivatives $(\gamma u_x, \gamma u_y)$ and $(\beta u_x, \beta u_y)$ respectively, such that (2.1) can be written into a first order system as follows:

$$\begin{cases} \boldsymbol{p} = \gamma \nabla u, \\ \boldsymbol{q} = \beta \nabla u, \\ u_{tt} = \nabla \cdot (\gamma \boldsymbol{p}) - \alpha u_t + \nabla \cdot (\beta \boldsymbol{q}_t). \end{cases} \tag{2.3}$$

The semi-discrete LDG method for (2.3) is formulated as: find $p_h^1, p_h^2, q_h^1, q_h^2, u_h \in V_h^k$ such that

$$\int_{K_{ij}} p_h^1 \phi d\boldsymbol{x} + \int_{K_{ij}} u_h (\gamma\phi)_x d\boldsymbol{x} - \int_{J_j} \widehat{u_h}\gamma^- \phi(x^-_{i+\frac{1}{2}}, y)dy + \int_{J_j} \widehat{u_h}\gamma^+ \phi(x^+_{i-\frac{1}{2}}, y)dy = 0, \tag{2.4}$$

$$\int_{K_{ij}} p_h^2 \varphi d\boldsymbol{x} + \int_{K_{ij}} u_h (\gamma\varphi)_y d\boldsymbol{x} - \int_{I_i} \widetilde{u_h}\gamma^- \varphi(x, y^-_{j+\frac{1}{2}})dx + \int_{I_i} \widetilde{u_h}\gamma^+ \varphi(x, y^+_{j-\frac{1}{2}})dx = 0, \tag{2.5}$$

$$\int_{K_{ij}} q_h^1 \zeta d\boldsymbol{x} + \int_{K_{ij}} u_h (\beta\zeta)_x d\boldsymbol{x} - \int_{J_j} \widehat{u_h}\beta^- \zeta(x^-_{i+\frac{1}{2}}, y)dy + \int_{J_j} \widehat{u_h}\beta^+ \zeta(x^+_{i-\frac{1}{2}}, y)dy = 0, \tag{2.6}$$

$$\int_{K_{ij}} q_h^2 \psi d\boldsymbol{x} + \int_{K_{ij}} u_h (\beta\psi)_y d\boldsymbol{x} - \int_{I_i} \widetilde{u_h}\beta^- \psi(x, y^-_{j+\frac{1}{2}})dx + \int_{I_i} \widetilde{u_h}\beta^+ \psi(x, y^+_{j-\frac{1}{2}})dx = 0, \tag{2.7}$$

$$\begin{aligned} &\int_{K_{ij}} (u_h)_{tt} w d\boldsymbol{x} + \int_{K_{ij}} \alpha (u_h)_t w d\boldsymbol{x} + \int_{K_{ij}} \gamma\big(p_h^1 w_x + p_h^2 w_y\big) d\boldsymbol{x} - \int_{J_j} \widehat{\gamma p_h^1} w(x^-_{i+\frac{1}{2}}, y)dy \\ &\quad + \int_{J_j} \widehat{\gamma p_h^1} w(x^+_{i-\frac{1}{2}}, y)dy - \int_{I_i} \widetilde{\gamma p_h^2} w(x, y^-_{j+\frac{1}{2}})dx + \int_{I_i} \widetilde{\gamma p_h^2} w(x, y^+_{j-\frac{1}{2}})dx \\ &\quad + \int_{K_{ij}} \beta\big((q_h^1)_t w_x + (q_h^2)_t w_y\big) d\boldsymbol{x} - \int_{J_j} \widehat{\beta(q_h^1)_t} w(x^-_{i+\frac{1}{2}}, y)dy + \int_{J_j} \widehat{\beta(q_h^1)_t} w(x^+_{i-\frac{1}{2}}, y)dy \\ &\quad - \int_{I_i} \widetilde{\beta(q_h^2)_t} w(x, y^-_{j+\frac{1}{2}})dx + \int_{I_i} \widetilde{\beta(q_h^2)_t} w(x, y^+_{j-\frac{1}{2}})dx = 0 \end{aligned} \tag{2.8}$$

for any test functions $\phi, \varphi, \zeta, \psi, w \in V_h^k$. The "hat" terms $\widehat{u_h}, \widehat{\gamma p_h^1}, \widehat{\beta q_h^1}$ and the "tilde" terms $\widetilde{u_h}, \widetilde{\gamma p_h^2}, \widetilde{\beta q_h^2}$ are cell boundary terms obtained from integration by parts, and they are the so-called numerical fluxes, which need to be defined suitably to ensure stability. Note that in (2.4)-(2.7), γ and β are not included in the numerical fluxes and take their own values from inside the cell K_{ij}, in the same way as the test functions. This choice of discretization can guarantee the continuity of u, see [6] for a more detailed explanation.

If $\beta(\boldsymbol{x})$ and $\gamma(\boldsymbol{x})$ are both continuous, then the numerical fluxes $\widehat{\gamma p_h^1}, \widehat{\beta q_h^1}$ and $\widetilde{\gamma p_h^2}, \widetilde{\beta q_h^2}$ can be reasonably defined. However, if they are discontinuous, these numerical fluxes should be carefully defined at the interface since the function (for example, $\beta(\boldsymbol{x})$) takes different values from both sides of the interface. The LDG method also becomes quite complicated to design if the discontinuities of $\beta(\boldsymbol{x})$ or $\gamma(\boldsymbol{x})$ occur inside an element. Hence here we assume that the discontinuities only occur in the direction aligned with the spatial discretization either vertical or horizontal or both, so that we can align the jumps with cell interfaces. Then for such a piecewise smooth function $a(\boldsymbol{x})$, we also define

$$|\nabla a|_\infty := \max_{K\in\mathcal{T}_h}\{\|\nabla a(\boldsymbol{x})\|_\infty |\ \boldsymbol{x}\in K\}.$$

Besides, we denote the L^2 norm over the domain Ω as $\|\cdot\|$ and denote the L^∞ norm as $\|\cdot\|_\infty$.

Theorem 2.1. *If the numerical fluxes are taken as the following alternating fluxes:*

$$\widehat{u_h} = \widetilde{u_h} = u_h^-, \quad \widehat{\gamma p_h^\ell} = \widetilde{\gamma p_h^\ell} = \gamma^+ (p_h^\ell)^+, \quad \widehat{\beta q_h^\ell} = \widetilde{\beta q_h^\ell} = \beta^+ (q_h^\ell)^+, \quad \ell = 1, 2, \tag{2.9}$$

or

$$\widehat{u_h} = \widetilde{u_h} = u_h^+, \quad \widehat{\gamma p_h^\ell} = \widetilde{\gamma p_h^\ell} = \gamma^- (p_h^\ell)^-, \quad \widehat{\beta q_h^\ell} = \widetilde{\beta q_h^\ell} = \beta^- (q_h^\ell)^-, \quad \ell = 1, 2, \tag{2.10}$$

then the semi-discrete LDG method presented in (2.4)-(2.8) *with periodic or homogeneous Dirichlet boundary conditions is energy stable, namely*

$$\frac{d}{dt}\int_{\mathcal{T}_h} \left[(u_h)_t^2 + |\boldsymbol{p}_h|^2\right] d\boldsymbol{x} \le 0,$$

where $\boldsymbol{p}_h = (p_h^1, p_h^2)$.

Proof. Here we just provide the proof for one of the choices of the numerical fluxes, i.e. (2.9). The analysis is similar for (2.10). For a simple presentation, we omit the subscript of the notation and denote the cell K_{ij} by K. Let $(\cdot,\cdot)_K$ denote the L^2 inner product, that is $(\boldsymbol{f},\boldsymbol{g})_K = \int_K \boldsymbol{f}\cdot\boldsymbol{g} d\boldsymbol{x}$.

We define

$$A_K^a(u_h, \boldsymbol{\phi}) = \left(a u_h, \nabla\cdot\boldsymbol{\phi}\right)_K + \left(u_h \nabla a, \boldsymbol{\phi}\right)_K - \left(a u_h^-, \boldsymbol{\phi}\cdot\boldsymbol{n}_K\right)_{\partial K}, \tag{2.11}$$

$$B_K^a(\boldsymbol{r}_h, w) = \big(a\boldsymbol{r}_h, \nabla w\big)_K - \big(a^+\boldsymbol{r}_h^+ \cdot \boldsymbol{n}_K, w\big)_{\partial K}, \tag{2.12}$$

where $a = a(\boldsymbol{x})$ is a piecewise smooth function (smooth inside K). Then the semi-discrete LDG method with the numerical fluxes (2.9) can be rewritten as

$$\big(\boldsymbol{p}_h, \boldsymbol{\phi}\big)_K + A_K^\gamma(u_h, \boldsymbol{\phi}) = 0, \tag{2.13}$$

$$\big(\boldsymbol{q}_h, \boldsymbol{\varphi}\big)_K + A_K^\beta(u_h, \boldsymbol{\varphi}) = 0, \tag{2.14}$$

$$\big((u_h)_{tt}, w\big)_K + \big(\alpha(u_h)_t, w\big)_K + B_K^\gamma(\boldsymbol{p}_h, w) + B_K^\beta\big((\boldsymbol{q}_h)_t, w\big) = 0. \tag{2.15}$$

By taking the time derivative of (2.13) and (2.14), and choosing the test functions to be $\boldsymbol{\phi} = \boldsymbol{p}_h, \boldsymbol{\varphi} = (\boldsymbol{q}_h)_t$, one obtains

$$\big((\boldsymbol{p}_h)_t, \boldsymbol{p}_h\big)_K + A_K^\gamma\big((u_h)_t, \boldsymbol{p}_h\big) = 0, \tag{2.16}$$

$$\big((\boldsymbol{q}_h)_t, (\boldsymbol{q}_h)_t\big)_K + A_K^\beta\big((u_h)_t, (\boldsymbol{q}_h)_t\big) = 0. \tag{2.17}$$

We take $w = (u_h)_t$ in (2.15), and then get

$$\big((u_h)_{tt}, (u_h)_t\big)_K + \big(\alpha(u_h)_t, (u_h)_t\big)_K + B_K^\gamma\big(\boldsymbol{p}_h, (u_h)_t\big) + B_K^\beta\big((\boldsymbol{q}_h)_t, (u_h)_t\big) = 0. \tag{2.18}$$

Adding up (2.16)-(2.18) yields

$$\begin{aligned} &\big((u_h)_{tt}, (u_h)_t\big)_K + \big(\alpha(u_h)_t, (u_h)_t\big)_K + B_K^\gamma\big(\boldsymbol{p}_h, (u_h)_t\big) + B_K^\beta\big((\boldsymbol{q}_h)_t, (u_h)_t\big) \\ &+ \big((\boldsymbol{p}_h)_t, \boldsymbol{p}_h\big)_K + A_K^\gamma\big((u_h)_t, \boldsymbol{p}_h\big) + \big((\boldsymbol{q}_h)_t, (\boldsymbol{q}_h)_t\big)_K + A_K^\beta\big((u_h)_t, (\boldsymbol{q}_h)_t\big) = 0. \end{aligned} \tag{2.19}$$

By using integration by parts and summing up over K, we get

$$\sum_{K\in\mathcal{T}_h} \big[A_K^\gamma\big((u_h)_t, \boldsymbol{p}_h\big) + B_K^\gamma\big(\boldsymbol{p}_h, (u_h)_t\big)\big] = \sum_{K\in\mathcal{T}_h} \Big[A_K^\beta\big((u_h)_t, (\boldsymbol{q}_h)_t\big) + B_K^\beta\big((\boldsymbol{q}_h)_t, (u_h)_t\big)\Big] = 0,$$

if the periodic or homogeneous boundary conditions are used. Therefore,

$$\big((u_h)_{tt}, (u_h)_t\big)_{\mathcal{T}_h} + \big(\alpha(u_h)_t, (u_h)_t\big)_{\mathcal{T}_h} + \big((\boldsymbol{p}_h)_t, \boldsymbol{p}_h\big)_{\mathcal{T}_h} + \big((\boldsymbol{q}_h)_t, (\boldsymbol{q}_h)_t\big)_{\mathcal{T}_h} = 0,$$

which leads to

$$\frac{1}{2}\frac{d}{dt}\int_{\mathcal{T}_h} \big[(u_h)_t^2 + |\boldsymbol{p}_h|^2\big] d\boldsymbol{x} = -\int_{\mathcal{T}_h} \big[\alpha(u_h)_t^2 + |(\boldsymbol{q}_h)_t|^2\big] d\boldsymbol{x} \le 0.$$

□

Physically, the energy $E = \int_\Omega \left(u_t^2 + \gamma^2 |\nabla u|^2\right) d\boldsymbol{x}$ decays in the diffusive-viscous wave equation (2.1) with proper boundary conditions. From the proof for Theorem 2.1, we can see that the proposed semi-discrete LDG method (2.13)-(2.15) indeed maintains this important physical property.

Theorem 2.2. *When the periodic or homogeneous boundary conditions are used in the semi-discrete LDG method* (2.13)-(2.15)*, the energy*

$$E_h(t) = \int_{\mathcal{T}_h} \left((u_h)_t^2 + |\boldsymbol{p}_h|^2\right) d\boldsymbol{x}$$

does not increase with time.

3 Error estimates

In this section, we derive the optimal error estimates for the LDG method formulated in (2.13)-(2.15). More specifically, we first study the error estimate in the energy norm and then the analysis will be extended to the L^2 norm.

3.1 Projections and inequalities

Here, we introduce the projections that will be utilized throughout the paper. We denote $P_h\omega$ as the L_2 projection of a function $\omega(x)$ into space V_h^k, that is:

$$(P_h\omega, \varphi)_K = (\omega, \varphi)_K, \quad \forall \varphi \in Q^k(K). \tag{3.1}$$

3.1.1 Projection in the one-dimensional case

In the one-dimensional case, we define the projection operator P_h^- as follows

$$(P_h^-\omega - \omega, \varphi)_{K_i} = 0, \quad \forall \varphi \in P^{k-1}(K_i) \quad \text{and} \quad P_h^-\omega(x_{i+\frac{1}{2}}^-) = \omega(x_{i+\frac{1}{2}}^-), \tag{3.2}$$

which means that P_h^- projects $\omega(x)$ into the piecewise polynomial space of degree k while taking the values of ω at the cell interface $x_{i+\frac{1}{2}}$. Similarly, P_h^+ is defined as

$$(P_h^+\omega - \omega, \varphi)_{K_i} = 0, \quad \forall \varphi \in P^{k-1}(K_i) \quad \text{and} \quad P_h^+\omega(x_{i-\frac{1}{2}}^+) = \omega(x_{i-\frac{1}{2}}^+). \tag{3.3}$$

3.1.2 Projection in the two-dimensional case

Since Cartesian meshes are used in this paper, we apply the tensor product of the projections in the one-dimensional case. On a rectangular cell $K_{ij} = I_i \times J_j$, the projection P_h^- is defined as

$$P_h^- = P_{hx}^- \otimes P_{hy}^-, \tag{3.4}$$

where P_{hx}^- and P_{hy}^- are the one-dimensional projections in the x- and y-direction respectively, defined in the same form as in (3.2). To be more specific, the explicit formulations for $P_h^-\omega$ on K_{ij} are demonstrated as follows:

$$\int_{K_{ij}} \big(P_h^-\omega(x,y) - \omega(x,y)\big)\phi(x,y)dxdy = 0, \tag{3.5a}$$

$$\int_{I_i} \big(P_h^-\omega(x,y^-_{j+\frac{1}{2}}) - \omega(x,y^-_{j+\frac{1}{2}})\big)\phi(x,y^-_{j+\frac{1}{2}})dx = 0, \tag{3.5b}$$

$$\int_{J_j} \big(P_h^-\omega(x^-_{i+\frac{1}{2}},y) - \omega(x^-_{i+\frac{1}{2}},y)\big)\phi(x^-_{i+\frac{1}{2}},y)dy = 0, \tag{3.5c}$$

$$P_h^-\omega(x^-_{i+\frac{1}{2}},y^-_{j+\frac{1}{2}}) = \omega(x^-_{i+\frac{1}{2}},y^-_{j+\frac{1}{2}}), \tag{3.5d}$$

for any $\phi \in Q^{k-1}(K_{ij})$.

Another projection $\boldsymbol{\Pi}_h^+$ for vector-valued functions $\boldsymbol{\rho} = (\rho_1, \rho_2)$ is defined as

$$\boldsymbol{\Pi}_h^+\boldsymbol{\rho} = \big(P_{hx}^+ \otimes P_{hy}\rho_1, P_{hx} \otimes P_{hy}^+\rho_2\big), \tag{3.6}$$

where P_{hx} and P_{hy} are the one-dimensional L^2 projections in the x- and y-directions respectively. For a scalar function ρ, it is easy to list explicitly the formulations for $\Pi_1^+\rho := P_{hx}^+ \otimes P_{hy}\rho$

$$\int_{K_{ij}} \big(\Pi_1^+\rho(x,y) - \rho(x,y)\big)\phi(x,y)dxdy = 0, \tag{3.7a}$$

$$\int_{J_j} \big(\Pi_1^+\omega(x^+_{i-\frac{1}{2}},y) - \omega(x^+_{i-\frac{1}{2}},y)\big)\phi(x^+_{i-\frac{1}{2}},y)dy = 0, \tag{3.7b}$$

for any $\phi \in P^{k-1}(I_i) \otimes P^k(J_j)$. Similarly, we can define the projection $\Pi_2^+ := P_{hx} \otimes P_{hy}^+$.

For any $\boldsymbol{\rho} \in [H^{k+1}(\Omega)]^2$, the restriction of $\boldsymbol{\Pi}_h^+\boldsymbol{\rho}$ to K_{ij} are elements of $[Q^k(K_{ij})]^2$ and satisfy

$$\int_{K_{ij}} \big(\boldsymbol{\rho} - \boldsymbol{\Pi}_h^+\boldsymbol{\rho}\big) \cdot \nabla\varphi dxdy = 0, \tag{3.8}$$

and

$$\int_{I_i} \varphi(x, y^+_{j-\frac{1}{2}}) \big(\boldsymbol{\rho}(x, y^+_{j-\frac{1}{2}}) - \boldsymbol{\Pi}^+_h \boldsymbol{\rho}(x, y^+_{j-\frac{1}{2}}) \big) \cdot \boldsymbol{n}_{K_{ij}} dx = 0, \tag{3.9}$$

$$\int_{J_j} \varphi(x^+_{i-\frac{1}{2}}, y) \big(\boldsymbol{\rho}(x^+_{i-\frac{1}{2}}, y) - \boldsymbol{\Pi}^+_h \boldsymbol{\rho}(x^+_{i-\frac{1}{2}}, y) \big) \cdot \boldsymbol{n}_{K_{ij}} dy = 0, \tag{3.10}$$

for any $\varphi \in Q^k(K_{ij})$.

3.1.3 Approximation properties of projections

For these projections defined above, we have the following approximation properties (see [6, 13]):

(i) For any $\omega \in H^{k+1}(\Omega)$ and $\boldsymbol{\rho} \in [H^{k+1}(\Omega)]^2$,

$$\|P_h \omega - \omega\| \le C h^{k+1} \|\omega\|_{H^{k+1}(\Omega)}, \tag{3.11}$$

$$\big\|P^{\pm}_h \omega - \omega\big\| \le C h^{k+1} \|\omega\|_{H^{k+1}(\Omega)}, \quad \big\|\boldsymbol{\Pi}^{\pm}_h \boldsymbol{\rho} - \boldsymbol{\rho}\big\| \le C h^{k+1} \|\boldsymbol{\rho}\|_{H^{k+1}(\Omega)}, \tag{3.12}$$

where C is independent of the mesh size h.

(ii) For $\omega \in H^{k+2}(\Omega), \boldsymbol{\rho} \in W^k_h$,

$$\Big| \big(\omega - P^-_h \omega), \nabla \cdot \boldsymbol{\rho}\big)_{\mathcal{T}_h} - \big(\omega - \widehat{P^-_h \omega}, \boldsymbol{\rho} \cdot \boldsymbol{n}_K\big)_{\mathcal{E}_h} \Big| \le C h^{k+1} \|\omega\|_{H^{k+2}(\Omega)} \|\boldsymbol{\rho}\|_{\Omega}, \tag{3.13}$$

where C is independent of the mesh size h, and the "hat" term is the numerical flux taking either the value from one side of the interface (namely inside or outside of the cell K) or some linear combination of the values from both sides of the interface.

3.2 Error estimate in the energy norm

To derive the error estimates, let us first denote the errors by

$$\begin{aligned} &e_u = u - u_h = \xi_u + \eta_u, \quad \xi_u = P^-_h u - u_h, \quad \eta_u = u - P^-_h u, \\ &e_{\boldsymbol{p}} = \boldsymbol{p} - \boldsymbol{p}_h = \xi_{\boldsymbol{p}} + \eta_{\boldsymbol{p}} \quad \xi_{\boldsymbol{p}} = \boldsymbol{\Pi}^+_h \boldsymbol{p} - \boldsymbol{p}_h, \quad \eta_{\boldsymbol{p}} = \boldsymbol{p} - \boldsymbol{\Pi}^+_h \boldsymbol{p}, \\ &e_{\boldsymbol{q}} = \boldsymbol{q} - \boldsymbol{q}_h = \xi_{\boldsymbol{q}} + \eta_{\boldsymbol{q}}, \quad \xi_{\boldsymbol{q}} = \boldsymbol{\Pi}^+_h \boldsymbol{q} - \boldsymbol{q}_h, \quad \eta_{\boldsymbol{q}} = \boldsymbol{q} - \boldsymbol{\Pi}^+_h \boldsymbol{q}. \end{aligned} \tag{3.14}$$

In particular, the projection $\boldsymbol{\Pi}_h^+$ degenerates into P_h^+ in the one-dimensional case. We also should remark that the signs of the projections $P_h^\pm$ and $\boldsymbol{\Pi}_h^\pm$ of $u, \boldsymbol{p}$ and $\boldsymbol{q}$ in (3.14) are consistent with the choice of the numerical fluxes in (2.9). Therefore, if the other set of numerical fluxes are chosen, the signs of $P_h^\pm$ and $\boldsymbol{\Pi}_h^\pm$ in (3.14) should be changed accordingly.

It is easy to verify that the errors of the proposed LDG method satisfy the following equations:

$$\big(e_{\boldsymbol{p}}, \boldsymbol{\phi}\big)_K + A_K^\gamma\big(e_u, \boldsymbol{\phi}\big) = 0, \tag{3.15}$$

$$\big(e_{\boldsymbol{q}}, \boldsymbol{\varphi}\big)_K + A_K^\beta\big(e_u, \boldsymbol{\varphi}\big) = 0, \tag{3.16}$$

$$\big((e_u)_{tt}, w\big)_K + \big(\alpha(e_u)_t, w\big)_K + B_K^\gamma\big(e_{\boldsymbol{p}}, w\big) + B_K^\beta\big((e_{\boldsymbol{q}})_t, w\big) = 0, \tag{3.17}$$

for any $\boldsymbol{\phi}, \boldsymbol{\varphi} \in W_h^k, w \in V_h^k$.

Initial conditions play an important role in the optimal error estimates of the proposed LDG method, so we need to choose suitable projections for the initial conditions. Note that we have two initial conditions in (2.2), one is for u and the other is for u_t. We take the initial condition $u_h(\boldsymbol{x}, 0)$ as $P_h^- u_0(\boldsymbol{x})$, which is consistent with the choice of the numerical fluxes in (2.9). For the other initial condition $(u_h)_t(\boldsymbol{x}, 0)$, we take the standard L^2 projection. Thus, we get the following lemma.

Lemma 3.1. *Suppose the initial conditions of the LDG method* (2.13)-(2.15) *are given by*

$$u_h(\boldsymbol{x}, 0) = P_h^- u(\boldsymbol{x}, 0), \quad (u_h)_t(\boldsymbol{x}, 0) = P_h u_t(\boldsymbol{x}, 0) \tag{3.18}$$

then the following error estimates hold

$$\|\xi_u(0)\| = 0, \quad \|\xi_{\boldsymbol{p}}(0)\| \le Ch^{k+1}, \quad \|\xi_{\boldsymbol{q}}(0)\| \le Ch^{k+1}, \quad \|(\xi_u)_t(0)\| \le Ch^{k+1}, \tag{3.19}$$

and

$$\big((e_u)_t(0), w\big)_K = 0 \quad \forall\ w \in Q^k(K). \tag{3.20}$$

Here and below, C stands for a generic constant, which does not depend on h but may depend on the norms of the initial condition or the exact solution.

Proof. Since $\xi_u(0) = P_h^- u(0) - u_h(0) = 0$, it is obvious to have $\|\xi_u\| = 0$. From (3.15) we have

$$\big(e_{\boldsymbol{p}}(0), \boldsymbol{\phi}\big)_K = -A_K^\gamma\big(e_u(0), \boldsymbol{\phi}\big) = -A_K^\gamma\big(\eta_u(0), \boldsymbol{\phi}\big),$$

for any $\boldsymbol{\phi} \in W_h^k$. Choosing $\boldsymbol{\phi} = \xi_{\boldsymbol{p}}(0)$ gives

$$\big(e_{\boldsymbol{p}}(0), \xi_{\boldsymbol{p}}(0)\big)_K = -A_K^\gamma\big(\eta_u(0), \xi_{\boldsymbol{p}}(0)\big).$$

Summing up over all cells and using the projection properties (3.11)-(3.13) yield

$$\begin{aligned}
\|\xi_{\boldsymbol{p}}(0)\|^2 &= -\big(\xi_{\boldsymbol{p}}(0), \eta_{\boldsymbol{p}}(0)\big)_{\mathcal{T}_h} - \sum_{K\in\mathcal{T}_h} A_K^\gamma\big(\eta_u(0), \xi_{\boldsymbol{p}}(0)\big) \\
&= -\big(\xi_{\boldsymbol{p}}(0), \eta_{\boldsymbol{p}}(0)\big)_{\mathcal{T}_h} + \big(\gamma\eta_u^-(0), \xi_{\boldsymbol{p}}(0)\cdot\boldsymbol{n}_K\big)_{\mathcal{E}_h} - \big(\gamma\eta_u(0), \nabla\cdot\xi_{\boldsymbol{p}}(0)\big)_{\mathcal{T}_h} \\
&\quad - \big(\eta_u(0)\nabla\gamma, \xi_{\boldsymbol{p}}(0)\big)_{\mathcal{T}_h} \\
&\le \|\xi_{\boldsymbol{p}}(0)\|\|\eta_{\boldsymbol{p}}(0)\| + Ch^{k+1}\|\gamma\|_\infty\|u(0)\|_{H^{k+2}}\|\xi_{\boldsymbol{p}}(0)\| + |\nabla\gamma|_\infty\|\eta_u(0)\|\|\xi_{\boldsymbol{p}}(0)\| \\
&\le Ch^{k+1}\|\xi_{\boldsymbol{p}}(0)\|,
\end{aligned}$$

which directly leads to

$$\|\xi_{\boldsymbol{p}}(0)\| \le Ch^{k+1}.$$

Similarly, we can also get $\|\xi_{\boldsymbol{q}}(0)\| \le Ch^{k+1}$. Furthermore, we have

$$\begin{aligned}
\|(\xi_u)_t(0)\| = \|P_h^- u_t(0) - (u_h)_t(0)\| &= \|P_h^- u_t(0) - u_t(0) + u_t(0) - (u_h)_t(0)\| \\
&\le \|P_h^- u_t(0) - u_t(0)\| + \|u_t(0) - (u_h)_t(0)\| \\
&= \|P_h^- u_t(0) - u_t(0)\| + \|u_t(0) - P_h u_t(0)\| \\
&\le Ch^{k+1}.
\end{aligned}$$

Obviously, the definition of the L^2 projection yields

$$\big((e_u)_t(0), w\big)_K = \big(u_t(0) - (u_h)_t(0), w\big)_K = \big(u_t(0) - P_h u_t(0), w\big)_K = 0,$$

for any test function $w \in Q^k(K)$. □

Remark 3.1. *We would like to note that this special choice of initial condition is not critical in the optimal convergence rate of the proposed LDG method. Also, some previous studies on LDG methods showed that the different choices of initial condition have little impact on the convergence or super-convergence results [5, 18, 20].*

Lemma 3.2. *Assuming that $u, \boldsymbol{v}$ are both smooth, $A_K^a(\eta_u, \boldsymbol{\varphi})$ and $B_K^a(\eta_{\boldsymbol{v}}, \phi)$ are defined as* (2.11) *and* (2.12)*, then we have*

$$|A_K^a(\eta_u, \boldsymbol{\varphi})| \le Ch^{k+1}\|\boldsymbol{\varphi}\|_{L^2(K)}, \quad |B_K^a(\eta_{\boldsymbol{v}}, \phi)| \le Ch^{k+1}\|\phi\|_{L^2(K)}. \tag{3.21}$$

where $a = a(\boldsymbol{x})$ is a piecewise smooth function (smooth inside K), $\boldsymbol{\varphi} \in W_h^k, \phi \in V_h^k$ and the constant C is independent of h.

Proof. Due to the formulation of $A_K^a(\eta_u, \boldsymbol{\varphi})$ in (2.11), one obtains

$$\begin{aligned}
|A_K^a(\eta_u, \boldsymbol{\varphi})| &= \big|\big(a\eta_u, \nabla\cdot\boldsymbol{\varphi}\big)_K + \big(\eta_u\nabla a, \boldsymbol{\varphi}\big)_K - \big(a\eta_u^-, \boldsymbol{\varphi}\cdot\boldsymbol{n}_K\big)_{\partial K}\big| \\
&\le \big|\big(a\eta_u, \nabla\cdot\boldsymbol{\varphi}\big)_K - \big(a\eta_u^-, \boldsymbol{\varphi}\cdot\boldsymbol{n}_K\big)_{\partial K}\big| + \big|\big(\eta_u\nabla a, \boldsymbol{\varphi}\big)_K\big| \\
&\le \|a\|_{L^\infty(\mathcal{T}_h)}\|\eta_u\|_{L^2(\mathcal{T}_h)}\|\boldsymbol{\varphi}\|_{L^2(K)} + |\nabla a|_\infty\|\eta_u\|_{L^2(\mathcal{T}_h)}\|\boldsymbol{\varphi}\|_{L^2(K)} \le Ch^{k+1}\|\boldsymbol{\varphi}\|_{L^2(K)},
\end{aligned}$$

where the approximation properties of projections presented in (3.11)-(3.13) are used.

According to (2.12), we have

$$B_K^a\big(\eta_{\boldsymbol{v}}, \phi\big) = \big(a\eta_{\boldsymbol{v}}, \nabla\phi\big)_K - \big(a^+\eta_{\boldsymbol{v}}^+\cdot\boldsymbol{n}_K, \phi\big)_{\partial K}.$$

By using the property of the projection $\boldsymbol{\Pi}_h^+$, for any constant a_0, it is easy to get

$$\big(a_0\eta_{\boldsymbol{v}}, \phi\big)_K = a_0\big(\eta_{\boldsymbol{v}}, \phi\big)_K = 0, \quad \big(a_0\eta_{\boldsymbol{v}}^+\cdot\boldsymbol{n}_K, \phi\big)_{\partial K} = a_0\big(\eta_{\boldsymbol{v}}^+\cdot\boldsymbol{n}_K, \phi\big)_{\partial K} = 0.$$

Therefore, we can obtain

$$\begin{aligned}
\big|B_K^a\big(\eta_{\boldsymbol{v}}, \phi\big)\big| &= \big|\big(a\eta_{\boldsymbol{v}}, \nabla\phi\big)_K - \big(a^+\eta_{\boldsymbol{v}}^+\cdot\boldsymbol{n}_K, \phi\big)_{\partial K}\big| \\
&= \big|\big((a-a_c)\eta_{\boldsymbol{v}}, \nabla\phi\big)_K - \big((a^+-a_c)\eta_{\boldsymbol{v}}^+\cdot\boldsymbol{n}_K, \phi\big)_{\partial K}\big| \\
&\le Ch\bigg(\big(|\eta_{\boldsymbol{v}}|, |\nabla\phi|\big)_K + \big(|\eta_{\boldsymbol{v}}^+\cdot\boldsymbol{n}_K|, |\phi|\big)_{\partial K}\bigg) \\
&\le Ch\|\eta_{\boldsymbol{v}}\|_{L^2(K)}\|\nabla\phi\|_{L^2(K)} + Ch\|\eta_{\boldsymbol{v}}^+\cdot\boldsymbol{n}_K\|_{L^2(\partial K)}\|\phi\|_{L^2(\partial K)} \\
&\le C\|\eta_{\boldsymbol{v}}\|_{L^2(K)}\|\phi\|_{L^2(K)} + Ch^{1/2}\|\phi\|_{L^2(K)}\|\eta_{\boldsymbol{v}}^+\cdot\boldsymbol{n}_K\|_{L^2(\partial K)} \\
&\le C\|\eta_{\boldsymbol{v}}\|_{L^2(\mathcal{T}_h)}\|\phi\|_{L^2(K)} + C\|\phi\|_{L^2(K)}\big(h^{1/2}\|\eta_{\boldsymbol{v}}\|_{L^2(\mathcal{T}_h)} + \|\eta_{\boldsymbol{v}}\|_{L^2(\mathcal{T}_h)}\big) \\
&\le Ch^{k+1}\|\phi\|_{L^2(K)},
\end{aligned}$$

where a_c denotes the value of $a(\boldsymbol{x})$ evaluated at the center of the cell K and the inverse and trace inequalities are used as follows

$$h\|\nabla\phi\|_{L^2(K)} \le C\|\phi\|_{L^2(K)}, \quad h^{1/2}\|\phi\|_{L^2(\partial K)} \le C\|\phi\|_{L^2(K)},$$
$$\|\eta_{\boldsymbol{v}}\cdot\boldsymbol{n}\|^2_{L^2(\partial K)} \le C\|\eta_v\|_{L^2(K)}\|\eta_{\boldsymbol{v}}\|_{H^1(K)}.$$

Here the constant C is independent of h. □

Based on the initial conditions (3.18), we have the following error estimate in the energy norm.

Theorem 3.1. *Let $\boldsymbol{p}, \boldsymbol{q}, u$ be the exact smooth solutions of the diffusive-viscous wave equation* (2.3)*, and $\boldsymbol{p}_h, \boldsymbol{q}_h, u_h$ be the numerical solutions of the semi-discrete LDG method* (2.13)-(2.15) *with the smooth initial conditions* (3.18) *and periodic or homogeneous Dirichlet boundary conditions, there hold the following error estimates:*

$$\|(e_u)_t\| \le Ch^{k+1}, \quad \|e_{\boldsymbol{p}}\| \le Ch^{k+1}, \quad \|e_{\boldsymbol{q}}\| \le Ch^{k+1}, \tag{3.22}$$

where the constant C only depends on α, β, γ, and the time t and the solution u, and is independent of the mesh size h.

Proof. Based on (3.14), the error equations (3.15)-(3.17) become

$$\big(\xi_{\boldsymbol{p}}, \boldsymbol{\phi}\big)_K + \big(\eta_{\boldsymbol{p}}, \boldsymbol{\phi}\big)_K + A_K^{\gamma}\big(\xi_u, \boldsymbol{\phi}\big) + A_K^{\gamma}\big(\eta_u, \boldsymbol{\phi}\big) = 0, \tag{3.23}$$
$$\big(\xi_{\boldsymbol{q}}, \boldsymbol{\varphi}\big)_K + \big(\eta_{\boldsymbol{q}}, \boldsymbol{\varphi}\big)_K + A_K^{\beta}\big(\xi_u, \boldsymbol{\varphi}\big) + A_K^{\beta}\big(\eta_u, \boldsymbol{\varphi}\big) = 0, \tag{3.24}$$
$$\begin{aligned}\big((\xi_u)_{tt}, w\big)_K + \big((\eta_u)_{tt}, w\big)_K + \big(\alpha(\xi_u)_t, w\big)_K + \big(\alpha(\eta_u)_t, w\big)_K + B_K^{\gamma}\big(\xi_{\boldsymbol{p}}, w\big) \\ + B_K^{\beta}\big((\xi_{\boldsymbol{q}})_t, w\big) + B_K^{\gamma}\big(\eta_{\boldsymbol{p}}, w\big) + B_K^{\beta}\big((\eta_{\boldsymbol{q}})_t, w\big) = 0.\end{aligned} \tag{3.25}$$

We first take the time derivative of (3.23) and (3.24) respectively, and then choose the test functions to be $\boldsymbol{\phi} = \xi_{\boldsymbol{p}}$ and $\boldsymbol{\varphi} = (\xi_{\boldsymbol{q}})_t$, which gives us

$$\big((\xi_{\boldsymbol{p}})_t, \xi_{\boldsymbol{p}}\big)_K + \big((\eta_{\boldsymbol{p}})_t, \xi_{\boldsymbol{p}}\big)_K + A_K^{\gamma}\big((\xi_u)_t, \xi_{\boldsymbol{p}}\big) + A_K^{\gamma}\big((\eta_u)_t, \xi_{\boldsymbol{p}}\big) = 0, \tag{3.26}$$
$$\big((\xi_{\boldsymbol{q}})_t, (\xi_{\boldsymbol{q}})_t\big)_K + \big((\eta_{\boldsymbol{q}})_t, (\xi_{\boldsymbol{q}})_t\big)_K + A_K^{\beta}\big((\xi_u)_t, (\xi_{\boldsymbol{q}})_t\big) + A_K^{\beta}\big((\eta_u)_t, (\xi_{\boldsymbol{q}})_t\big) = 0. \tag{3.27}$$

Besides, choosing $w = (\xi_u)_t$ in (3.25) yields

$$\begin{aligned}\big((\xi_u)_{tt},(\xi_u)_t\big)_K + \big((\eta_u)_{tt},(\xi_u)_t\big)_K + \big(\alpha(\xi_u)_t,(\xi_u)_t\big)_K + \big(\alpha(\eta_u)_t,(\xi_u)_t\big)_K + B_K^{\gamma}\big(\xi_{\boldsymbol{p}},(\xi_u)_t\big)\\ + B_K^{\beta}\big((\xi_{\boldsymbol{q}})_t,(\xi_u)_t\big) + B_K^{\gamma}\big(\eta_{\boldsymbol{p}},(\xi_u)_t\big) + B_K^{\beta}\big((\eta_{\boldsymbol{q}})_t,(\xi_u)_t\big) = 0.\end{aligned} \tag{3.28}$$

Addition of (3.26)-(3.28) becomes

$$\begin{aligned}&\big((\xi_u)_{tt},(\xi_u)_t\big)_K + \big(\alpha(\xi_u)_t,(\xi_u)_t\big)_K + \big((\xi_{\boldsymbol{p}})_t,\xi_{\boldsymbol{p}}\big)_K + \big((\xi_{\boldsymbol{q}})_t,(\xi_{\boldsymbol{q}})_t\big)_K\\ =&-\big((\eta_u)_{tt},(\xi_u)_t\big)_K - \big(\alpha(\eta_u)_t,(\xi_u)_t\big)_K - \big((\eta_{\boldsymbol{p}})_t,\xi_{\boldsymbol{p}}\big)_K - \big((\eta_{\boldsymbol{q}})_t,(\xi_{\boldsymbol{q}})_t\big)_K\\ &- A_K^{\gamma}\big((\xi_u)_t,\xi_{\boldsymbol{p}}\big) - A_K^{\gamma}\big((\eta_u)_t,\xi_{\boldsymbol{p}}\big) - A_K^{\beta}\big((\xi_u)_t,(\xi_{\boldsymbol{q}})_t\big) - A_K^{\beta}\big((\eta_u)_t,(\xi_{\boldsymbol{q}})_t\big)\\ &- B_K^{\gamma}\big(\xi_{\boldsymbol{p}},(\xi_u)_t\big) - B_K^{\beta}\big((\xi_{\boldsymbol{q}})_t,(\xi_u)_t\big) - B_K^{\gamma}\big(\eta_{\boldsymbol{p}},(\xi_u)_t\big) - B_K^{\beta}\big((\eta_{\boldsymbol{q}})_t,(\xi_u)_t\big).\end{aligned}$$

By summing up the above equation over all cells and using integration by parts, we get

$$\begin{aligned}&\big((\xi_u)_{tt},(\xi_u)_t\big)_{\mathcal{T}_h} + \big(\alpha(\xi_u)_t,(\xi_u)_t\big)_{\mathcal{T}_h} + \big((\xi_{\boldsymbol{p}})_t,\xi_{\boldsymbol{p}}\big)_{\mathcal{T}_h} + \big((\xi_{\boldsymbol{q}})_t,(\xi_{\boldsymbol{q}})_t\big)_{\mathcal{T}_h}\\ =&-\big((\eta_u)_{tt},(\xi_u)_t\big)_{\mathcal{T}_h} - \big(\alpha(\eta_u)_t,(\xi_u)_t\big)_{\mathcal{T}_h} - \big((\eta_{\boldsymbol{p}})_t,\xi_{\boldsymbol{p}}\big)_{\mathcal{T}_h} - \big((\eta_{\boldsymbol{q}})_t,(\xi_{\boldsymbol{q}})_t\big)_{\mathcal{T}_h}\\ &-\sum_{K\in\mathcal{T}_h}\Big[A_K^{\gamma}\big((\eta_u)_t,\xi_{\boldsymbol{p}}\big) + A_K^{\beta}\big((\eta_u)_t,(\xi_{\boldsymbol{q}})_t\big) + B_K^{\gamma}\big(\eta_{\boldsymbol{p}},(\xi_u)_t\big) + B_K^{\beta}\big((\eta_{\boldsymbol{q}})_t,(\xi_u)_t\big)\Big]\end{aligned}$$

if periodic or homogeneous Dirichlet boundary conditions are used.

With the error estimates (3.21) in Lemma 3.2, one obtains

$$\left|\sum_{K\in\mathcal{T}_h} A_K^{\gamma}\big((\eta_u)_t,\xi_{\boldsymbol{p}}\big)\right| \le \sum_{K\in\mathcal{T}_h}\big|A_K^{\gamma}\big((\eta_u)_t,\xi_{\boldsymbol{p}}\big)\big| \le Ch^{k+1}\|\xi_{\boldsymbol{p}}\|, \tag{3.29}$$

$$\left|\sum_{K\in\mathcal{T}_h} A_K^{\beta}\big((\eta_u)_t,(\xi_{\boldsymbol{q}})_t\big)\right| \le \sum_{K\in\mathcal{T}_h}\Big|A_K^{\beta}\big((\eta_u)_t,(\xi_{\boldsymbol{q}})_t\big)\Big| \le Ch^{k+1}\|(\xi_{\boldsymbol{q}})_t\|, \tag{3.30}$$

$$\left|\sum_{K\in\mathcal{T}_h} B_K^{\gamma}\big(\eta_{\boldsymbol{p}},(\xi_u)_t\big)\right| \le \sum_{K\in\mathcal{T}_h}\big|B_K^{\gamma}\big(\eta_{\boldsymbol{p}},(\xi_u)_t\big)\big| \le Ch^{k+1}\|(\xi_u)_t\|, \tag{3.31}$$

$$\left|\sum_{K\in\mathcal{T}_h} B_K^{\beta}\big((\eta_{\boldsymbol{q}})_t,(\xi_u)_t\big)\right| \le \sum_{K\in\mathcal{T}_h}\Big|B_K^{\beta}\big((\eta_{\boldsymbol{q}})_t,(\xi_u)_t\big)\Big| \le Ch^{k+1}\|(\xi_u)_t\|. \tag{3.32}$$

Then by using the properties of the projections (3.12) and (3.13), we have

$$\begin{aligned}
&\frac{1}{2}\frac{d}{dt}\big(\|(\xi_u)_t\|^2+\|\xi_{\boldsymbol{p}}\|^2\big)+\|(\xi_{\boldsymbol{q}})_t\|^2+\|\alpha^{\frac{1}{2}}(\xi_u)_t\|^2\\
\le\ &\Big|\big((\eta_{\boldsymbol{p}})_t,\xi_{\boldsymbol{p}}\big)_{\mathcal{T}_h}\Big|+\Big|\big((\eta_u)_{tt},(\xi_u)_t\big)_{\mathcal{T}_h}\Big|+\Big|\big(\alpha^{\frac{1}{2}}(\eta_u)_t,\alpha^{\frac{1}{2}}(\xi_u)_t\big)_{\mathcal{T}_h}\Big|+\Big|\big((\eta_{\boldsymbol{q}})_t,(\xi_{\boldsymbol{q}})_t\big)_{\mathcal{T}_h}\Big|\\
&+\left|\sum_{K\in\mathcal{T}_h}\Big[A_K^{\gamma}\big((\eta_u)_t,\xi_{\boldsymbol{p}}\big)+A_K^{\beta}\big((\eta_u)_t,(\xi_{\boldsymbol{q}})_t\big)+B_K^{\gamma}\big(\eta_{\boldsymbol{p}},(\xi_u)_t\big)+B_K^{\beta}\big((\eta_{\boldsymbol{q}})_t,(\xi_u)_t\big)\Big]\right|\\
\le\ &Ch^{k+1}\big(\|\xi_{\boldsymbol{p}}\|+\|(\xi_u)_t\|+\|(\xi_{\boldsymbol{q}})_t\|+\|\alpha^{\frac{1}{2}}(\xi_u)_t\|\big)\\
\le\ &\|(\xi_u)_t\|^2+\|\xi_{\boldsymbol{p}}\|^2+\|(\xi_{\boldsymbol{q}})_t\|^2+\|\alpha^{\frac{1}{2}}(\xi_u)_t\|^2+Ch^{2k+2},
\end{aligned}$$

which leads to

$$\frac{d}{dt}\big(\|(\xi_u)_t\|^2+\|\xi_{\boldsymbol{p}}\|^2\big)\le\|(\xi_u)_t\|^2+\|\xi_{\boldsymbol{p}}\|^2+Ch^{2k+2}.$$

Combing this inequality with the approximation of the initial condition (3.19), we can conclude that

$$\|(\xi_u)_t\|^2+\|\xi_{\boldsymbol{p}}\|^2\le Ch^{2k+2},$$

which leads to

$$\|(\xi_u)_t\|^2\le Ch^{2k+2},\quad \|\xi_{\boldsymbol{p}}\|^2\le Ch^{2k+2}.$$

Together the property of the projection (3.12), we complete the error estimate as follows

$$\|(e_u)_t\|\le Ch^{k+1},\quad \|e_{\boldsymbol{p}}\|\le Ch^{k+1}$$

where the constant C is independent of the mesh size h. Furthermore, since $e_{\boldsymbol{p}}=\gamma\nabla e_u, e_{\boldsymbol{q}}=\beta\nabla e_u$, we can obtain

$$\|e_{\boldsymbol{q}}\|=\left\|\frac{\beta}{\gamma}e_{\boldsymbol{p}}\right\|\le\left\|\frac{\beta}{\gamma}\right\|_{\infty}\|e_{\boldsymbol{p}}\|\le Ch^{k+1}.$$

□

3.3 Error estimate in the L^2 norm

In this subsection, we give the error estimate in the L^2 norm.

Theorem 3.2. *Let $\boldsymbol{p},\boldsymbol{q},u$ be the exact smooth solutions of the diffusive-viscous wave equation* (2.3)*, and $\boldsymbol{p}_h,\boldsymbol{q}_h,u_h$ be the numerical solutions of the semi-discrete LDG method* (2.13)-(2.15)

with the smooth initial conditions (3.18) *and periodic or homogeneous Dirichlet boundary conditions, there hold the following error estimate:*

$$\max_{t\in[0,T]} \|e_u(t)\| \le Ch^{k+1}, \tag{3.33}$$

where the constant C only depends on α, β, γ , the time T and the solution u, and is independent of the mesh size h.

Proof. By using product rule for the time derivative in (3.25), we can obtain

$$\begin{aligned} &-\big((\xi_u)_t, w_t\big)_K + \big(\alpha(\xi_u)_t, w\big)_K + B_K^{\gamma}\big(\xi_{\boldsymbol{p}}, w\big) + B_K^{\beta}\big((\xi_{\boldsymbol{q}})_t, w\big) \\ &\quad = -\big((\eta_u)_{tt}, w\big)_K - \big(\alpha(\eta_u)_t, w\big)_K - B_K^{\gamma}\big(\eta_{\boldsymbol{p}}, w\big) - B_K^{\beta}\big((\eta_{\boldsymbol{q}})_t, w\big) - \frac{d}{dt}\big((\xi_u)_t, w\big)_K. \end{aligned} \tag{3.34}$$

For any fixed time $\tau \le T$, let us denote the time integral of the error by

$$\begin{aligned} E_u(t) &= \int_t^{\tau} e_u(s)ds, \quad E_u^{\xi}(t) = \int_t^{\tau} \xi_u(s)ds, \quad E_u^{\eta}(t) = \int_t^{\tau} \eta_u(s)ds, \\ E_{\boldsymbol{p}}(t) &= \int_t^{\tau} e_{\boldsymbol{p}}(s)ds, \quad E_{\boldsymbol{p}}^{\xi}(t) = \int_t^{\tau} \xi_{\boldsymbol{p}}(s)ds, \quad E_{\boldsymbol{p}}^{\eta}(t) = \int_t^{\tau} \eta_{\boldsymbol{p}}(s)ds, \\ E_{\boldsymbol{q}}(t) &= \int_t^{\tau} e_{\boldsymbol{q}}(s)ds, \quad E_{\boldsymbol{q}}^{\xi}(t) = \int_t^{\tau} \xi_{\boldsymbol{q}}(s)ds, \quad E_{\boldsymbol{q}}^{\eta}(t) = \int_t^{\tau} \eta_{\boldsymbol{q}}(s)ds. \end{aligned}$$

Integrating (3.15) and (3.16) in time from t to τ give us

$$\big(E_{\boldsymbol{p}}, \boldsymbol{\phi}\big)_K + A_K^{\gamma}\big(E_u, \boldsymbol{\phi}\big) = 0, \tag{3.35}$$

$$\big(E_{\boldsymbol{q}}, \boldsymbol{\varphi}\big)_K + A_K^{\beta}\big(E_u, \boldsymbol{\varphi}\big) = 0. \tag{3.36}$$

Taking $w = E_u^{\xi}, \boldsymbol{\phi} = \xi_{\boldsymbol{p}}, \boldsymbol{\varphi} = (\xi_{\boldsymbol{q}})_t$ in (3.34)-(3.36), and using the fact that $w_t = -\xi_u$, we can get

$$\begin{aligned} &\big((\xi_u)_t, \xi_u\big)_K + \big(\alpha(\xi_u)_t, E_u^{\xi}\big)_K + B_K^{\gamma}\big(\xi_{\boldsymbol{p}}, E_u^{\xi}\big) + B_K^{\beta}\big((\xi_{\boldsymbol{q}})_t, E_u^{\xi}\big) \\ &= -\big((\eta_u)_{tt}, E_u^{\xi}\big)_K - \big(\alpha(\eta_u)_t, E_u^{\xi}\big)_K - B_K^{\gamma}\big(\eta_{\boldsymbol{p}}, E_u^{\xi}\big) - B_K^{\beta}\big((\eta_{\boldsymbol{q}})_t, E_u^{\xi}\big) - \frac{d}{dt}\big((\xi_u)_t, E_u^{\xi}\big)_K, \end{aligned} \tag{3.37}$$

$$\big(E_{\boldsymbol{p}}^{\xi}, \xi_{\boldsymbol{p}}\big)_K + A_K^{\gamma}\big(E_u^{\xi}, \xi_{\boldsymbol{p}}\big) = -\big(E_{\boldsymbol{p}}^{\eta}, \xi_{\boldsymbol{p}}\big)_K - A_K^{\gamma}\big(E_u^{\eta}, \xi_{\boldsymbol{p}}\big), \tag{3.38}$$

$$\big(E_{\boldsymbol{q}}^{\xi}, (\xi_{\boldsymbol{q}})_t\big)_K + A_K^{\beta}\big(E_u^{\xi}, (\xi_{\boldsymbol{q}})_t\big) = -\big(E_{\boldsymbol{q}}^{\eta}, (\xi_{\boldsymbol{q}})_t\big)_K - A_K^{\beta}\big(E_u^{\eta}, (\xi_{\boldsymbol{q}})_t\big). \tag{3.39}$$

Summing up (3.37)-(3.39) over all cells and using integration by parts, and using periodic or homogeneous Dirichlet boundary conditions, one has

$$\begin{aligned}\frac{1}{2}\frac{d}{dt}\left(\|\xi_u\|^2-\|E_{\boldsymbol{p}}^{\xi}\|^2\right)=&-\big((\eta_u)_{tt},E_u^{\xi}\big)_{\mathcal{T}_h}-\big(\alpha(\eta_u)_t,E_u^{\xi}\big)_{\mathcal{T}_h}-\frac{d}{dt}\big((\xi_u)_t,E_u^{\xi}\big)_{\mathcal{T}_h}\\&-\big(\alpha(\xi_u)_t,E_u^{\xi}\big)_{\mathcal{T}_h}-\big(E_{\boldsymbol{q}}^{\xi},(\xi_{\boldsymbol{q}})_t\big)_{\mathcal{T}_h}-\big(E_{\boldsymbol{p}}^{\eta},\xi_{\boldsymbol{p}}\big)_{\mathcal{T}_h}-\big(E_{\boldsymbol{q}}^{\eta},(\xi_{\boldsymbol{q}})_t\big)_{\mathcal{T}_h}\\&-\sum_{K\in\mathcal{T}_h}\Big[A_K^{\gamma}\big(E_u^{\eta},\xi_{\boldsymbol{p}}\big)+A_K^{\beta}\big(E_u^{\eta},(\xi_{\boldsymbol{q}})_t\big)+B_K^{\gamma}\big(\eta_{\boldsymbol{p}},E_u^{\xi}\big)+B_K^{\beta}\big((\eta_{\boldsymbol{q}})_t,E_u^{\xi}\big)\Big].\end{aligned}\tag{3.40}$$

Integrating (3.40) from 0 to τ and using the fact that $E_u^{\xi}(\tau)=E_{\boldsymbol{p}}^{\xi}(\tau)=0$, one gets

$$\begin{aligned}&\frac{1}{2}\|\xi_u(\tau)\|^2-\frac{1}{2}\|\xi_u(0)\|^2+\frac{1}{2}\|E_{\boldsymbol{p}}^{\xi}(0)\|^2\\&=-\int_0^{\tau}\big((\eta_u)_{tt},E_u^{\xi}\big)_{\mathcal{T}_h}dt-\int_0^{\tau}\big(\alpha(\xi_u)_t,E_u^{\xi}\big)_{\mathcal{T}_h}dt+\big((\xi_u)_t(0),E_u^{\xi}(0)\big)_{\mathcal{T}_h}\\&\quad-\int_0^{\tau}\big(\alpha(\eta_u)_t,E_u^{\xi}\big)_{\mathcal{T}_h}dt-\int_0^{\tau}\big(E_{\boldsymbol{q}}^{\xi},(\xi_{\boldsymbol{q}})_t\big)_{\mathcal{T}_h}dt-\int_0^{\tau}\big(E_{\boldsymbol{p}}^{\eta},\xi_{\boldsymbol{p}}\big)_{\mathcal{T}_h}dt-\int_0^{\tau}\big(E_{\boldsymbol{q}}^{\eta},(\xi_{\boldsymbol{q}})_t\big)_{\mathcal{T}_h}dt\\&\quad-\sum_{K\in\mathcal{T}_h}\int_0^{\tau}\Big[A_K^{\gamma}\big(E_u^{\eta},\xi_{\boldsymbol{p}}\big)+A_K^{\beta}\big(E_u^{\eta},(\xi_{\boldsymbol{q}})_t\big)+B_K^{\gamma}\big(\eta_{\boldsymbol{p}},E_u^{\xi}\big)+B_K^{\beta}\big((\eta_{\boldsymbol{q}})_t,E_u^{\xi}\big)\Big]dt.\end{aligned}\tag{3.41}$$

Moreover, by using integration by parts in time, we can get

$$\begin{aligned}&\int_0^{\tau}\big((\eta_u)_{tt},E_u^{\xi}\big)_{\mathcal{T}_h}dt=\int_{\mathcal{T}_h}\int_0^{\tau}(\eta_u)_{tt}E_u^{\xi}dtd\boldsymbol{x}=-\big((\eta_u)_t(0),E_u^{\xi}(0)\big)_{\mathcal{T}_h}+\int_0^{\tau}\big(\xi_u,(\eta_u)_t\big)_{\mathcal{T}_h}dt,\\&\int_0^{\tau}\big(\alpha(\xi_u)_t,E_u^{\xi}\big)_{\mathcal{T}_h}dt=\int_{\mathcal{T}_h}\int_0^{\tau}(\xi_u)_tE_u^{\xi}dtd\boldsymbol{x}=-\big(\alpha\xi_u(0),E_u^{\xi}(0)\big)_{\mathcal{T}_h}+\int_0^{\tau}\|\xi_u\|^2dt,\\&\int_0^{\tau}\big(\alpha(\eta_u)_t,E_u^{\xi}\big)_{\mathcal{T}_h}dt=\int_{\mathcal{T}_h}\int_0^{\tau}\alpha(\eta_u)_tE_u^{\xi}dt\boldsymbol{x}=-\big(\alpha\eta_u(0),E_u^{\xi}(0)\big)_{\mathcal{T}_h}+\int_0^{\tau}\big(\xi_u,\eta_u\big)_{\mathcal{T}_h}dt,\\&\int_0^{\tau}\big(E_{\boldsymbol{q}}^{\xi},(\xi_{\boldsymbol{q}})_t\big)_{\mathcal{T}_h}dt=\int_{\mathcal{T}_h}\int_0^{\tau}E_{\boldsymbol{q}}^{\xi}\cdot(\xi_{\boldsymbol{q}})_tdtd\boldsymbol{x}=-\big(E_{\boldsymbol{q}}^{\xi}(0),\xi_{\boldsymbol{q}}(0)\big)_{\mathcal{T}_h}+\int_0^{\tau}\|\xi_{\boldsymbol{q}}\|^2dt,\\&\int_0^{\tau}\big(E_{\boldsymbol{q}}^{\eta},(\xi_{\boldsymbol{q}})_t\big)_{\mathcal{T}_h}dt=\int_{\mathcal{T}_h}\int_0^{\tau}E_{\boldsymbol{q}}^{\eta}\cdot(\xi_{\boldsymbol{q}})_tdtd\boldsymbol{x}=-\big(E_{\boldsymbol{q}}^{\eta}(0),\xi_{\boldsymbol{q}}(0)\big)_{\mathcal{T}_h}+\int_0^{\tau}\big(\xi_{\boldsymbol{q}},\eta_{\boldsymbol{q}}\big)_{\mathcal{T}_h}dt,\\&\int_0^{\tau}A_K^{\beta}\big(E_u^{\eta},(\xi_{\boldsymbol{q}})_t\big)dt=\int_K\int_0^{\tau}E_u^{\eta}\big[\beta\nabla\cdot(\xi_{\boldsymbol{q}})_t+\nabla\beta\cdot(\xi_{\boldsymbol{q}})_t\big]dtd\boldsymbol{x}-\int_{\partial K}\int_0^{\tau}\beta(E_u^{\eta})^{-}(\xi_{\boldsymbol{q}})_t\cdot\boldsymbol{n}_Kdtds\\&\qquad=-A_K^{\beta}\big(E_u^{\eta}(0),\xi_{\boldsymbol{q}}(0)\big)+\int_0^{\tau}A_K^{\beta}\big(\eta_u,\xi_{\boldsymbol{q}}\big)dt.\end{aligned}$$

Plugging these above equations into (3.41) and combing with the properties of the L^2 projection

(3.19) and (3.20), one obtains

$$
\begin{aligned}
&\frac{1}{2}\|\xi_u(\tau)\|^2-\frac{1}{2}\|\xi_u(0)\|^2+\frac{1}{2}\|E_{\boldsymbol{p}}^{\xi}(0)\|^2\\
&=\big((e_u)_t(0),E_u^{\xi}(0)\big)_{\mathcal{T}_h}-\int_0^{\tau}\big(\xi_u,(\eta_u)_t\big)_{\mathcal{T}_h}dt+\big(\alpha\xi_u(0),E_u^{\xi}(0)\big)_{\mathcal{T}_h}-\int_0^{\tau}\|\xi_u\|^2dt\\
&\quad+\big(\alpha\eta_u(0),E_u^{\xi}(0)\big)_{\mathcal{T}_h}-\int_0^{\tau}\big(\xi_u,\eta_u\big)_{\mathcal{T}_h}dt-\int_0^{\tau}\big(E_{\boldsymbol{p}}^{\eta},\xi_{\boldsymbol{p}}\big)_{\mathcal{T}_h}dt+\big(E_{\boldsymbol{q}}^{\xi}(0),\xi_{\boldsymbol{q}}(0)\big)_{\mathcal{T}_h}-\int_0^{\tau}\|\xi_{\boldsymbol{q}}\|^2dt\\
&\quad+\big(E_{\boldsymbol{q}}^{\eta}(0),\xi_{\boldsymbol{q}}(0)\big)_{\mathcal{T}_h}-\int_0^{\tau}\big(\xi_{\boldsymbol{q}},\eta_{\boldsymbol{q}}\big)_{\mathcal{T}_h}dt+\sum_{K\in\mathcal{T}_h}A_K^{\beta}\big(E_u^{\eta}(0),\xi_{\boldsymbol{q}}(0)\big)-\sum_{K\in\mathcal{T}_h}\int_0^{\tau}A_K^{\beta}\big(\eta_u,\xi_{\boldsymbol{q}}\big)dt\\
&\quad-\sum_{K\in\mathcal{T}_h}\int_0^{\tau}A_K^{\gamma}\big(E_u^{\eta},\xi_{\boldsymbol{p}}\big)dt-\sum_{K\in\mathcal{T}_h}\int_0^{\tau}B_K^{\gamma}\big(\eta_{\boldsymbol{p}},E_u^{\xi}\big)-\sum_{K\in\mathcal{T}_h}\int_0^{\tau}B_K^{\beta}\big((\eta_{\boldsymbol{q}})_t,E_u^{\xi}\big)\\
&=-\int_0^{\tau}\big(\xi_u,(\eta_u)_t\big)_{\mathcal{T}_h}dt-\int_0^{\tau}\|\xi_u\|^2dt+\big(\alpha\eta_u(0),E_u^{\xi}(0)\big)_{\mathcal{T}_h}-\int_0^{\tau}\big(\xi_u,\eta_u\big)_{\mathcal{T}_h}dt-\int_0^{\tau}\big(\xi_{\boldsymbol{q}},\eta_{\boldsymbol{q}}\big)_{\mathcal{T}_h}dt\\
&\quad-\int_0^{\tau}\big(E_{\boldsymbol{p}}^{\eta},\xi_{\boldsymbol{p}}\big)_{\mathcal{T}_h}dt+\big(E_{\boldsymbol{q}}^{\xi}(0),\xi_{\boldsymbol{q}}(0)\big)_{\mathcal{T}_h}+\big(E_{\boldsymbol{q}}^{\eta}(0),\xi_{\boldsymbol{q}}(0)\big)_{\mathcal{T}_h}-\int_0^{\tau}\|\xi_{\boldsymbol{q}}\|^2dt+\sum_{K\in\mathcal{T}_h}A_K^{\beta}\big(E_u^{\eta}(0),\xi_{\boldsymbol{q}}(0)\big)\\
&\quad-\sum_{K\in\mathcal{T}_h}\int_0^{\tau}\Big(A_K^{\beta}\big(\eta_u,\xi_{\boldsymbol{q}}\big)+A_K^{\gamma}\big(E_u^{\eta},\xi_{\boldsymbol{p}}\big)+B_K^{\gamma}\big(\eta_{\boldsymbol{p}},E_u^{\xi}\big)+B_K^{\beta}\big((\eta_{\boldsymbol{q}})_t,E_u^{\xi}\big)\Big)dt.
\end{aligned}
$$

We notice that

$$
\begin{aligned}
E_u^{\eta}(t)&=\int_t^{\tau}\eta_u(s)ds=\int_t^{\tau}\big(u(s)-P_h^{-}u(s)\big)ds=\int_t^{\tau}u(s)ds-P_h^{-}\left(\int_t^{\tau}u(s)ds\right),\\
E_{\boldsymbol{p}}^{\eta}(t)&=\int_t^{\tau}\eta_{\boldsymbol{p}}(s)ds=\int_t^{\tau}\big(\boldsymbol{p}(s)-\boldsymbol{\Pi}_h^{+}\boldsymbol{p}(s)\big)ds=\int_t^{\tau}\boldsymbol{p}(s)ds-\boldsymbol{\Pi}_h^{+}\left(\int_t^{\tau}\boldsymbol{p}(s)ds\right),\\
E_{\boldsymbol{q}}^{\eta}(t)&=\int_t^{\tau}\eta_{\boldsymbol{q}}(s)ds=\int_t^{\tau}\big(\boldsymbol{q}(s)-\boldsymbol{\Pi}_h^{+}\boldsymbol{q}(s)\big)ds=\int_t^{\tau}\boldsymbol{q}(s)ds-\boldsymbol{\Pi}_h^{+}\left(\int_t^{\tau}\boldsymbol{q}(s)ds\right).
\end{aligned}
$$

By the properties of the projections P_h^{-} and $\boldsymbol{\Pi}_h^{+}$ in (3.12), we have

$$
\|E_u^{\eta}\|\le Ch^{k+1},\quad \|E_{\boldsymbol{p}}^{\eta}\|\le Ch^{k+1},\quad \|E_{\boldsymbol{q}}^{\eta}\|\le Ch^{k+1}.
$$

Due to the property of the projection P_h^{-} in (3.13), we also have

$$
\begin{aligned}
&\left|\sum_{K\in\mathcal{T}_h}A_K^{\beta}\big(E_u^{\eta}(0),\xi_{\boldsymbol{q}}(0)\big)\right|\le\big(Ch^{k+1}+|\nabla\beta|_{\infty}\|E_u^{\eta}(0)\|\big)\,\|\xi_{\boldsymbol{q}}(0)\|\le Ch^{2k+2},\\
&\left|\sum_{K\in\mathcal{T}_h}A_K^{\gamma}\big(E_u^{\eta},\xi_{\boldsymbol{p}}\big)\right|\le\big(Ch^{k+1}+|\nabla\gamma|_{\infty}\|E_u^{\eta}\|\big)\|\xi_{\boldsymbol{p}}\|\le Ch^{2k+2},\\
&\left|\sum_{K\in\mathcal{T}_h}A_K^{\beta}\big(\eta_u,\xi_{\boldsymbol{q}}\big)\right|\le\big(Ch^{k+1}+|\nabla\beta|_{\infty}\|E_u^{\eta}\|\big)\|\xi_{\boldsymbol{q}}\|\le Ch^{2k+2},
\end{aligned}
$$

$$\left|\sum_{K\in\mathcal{T}_h} B_K^{\gamma}\big(\eta_{\boldsymbol{p}}, E_u^{\xi}\big)\right| \le Ch^{k+1}\|E_u^{\xi}\|, \qquad \left|\sum_{K\in\mathcal{T}_h} B_K^{\beta}\big((\eta_{\boldsymbol{q}})_t, E_u^{\xi}\big)\right| \le Ch^{k+1}\|E_u^{\xi}\|,$$

where we use the error estimate result of $\boldsymbol{p}$ and $\boldsymbol{q}$ in (3.22) and Lemma 3.2.

With these inequalities above, we finally obtain

$$\begin{aligned}
&\frac{1}{2}\|\xi_u(\tau)\|^2 - \frac{1}{2}\|\xi_u(0)\|^2 + \frac{1}{2}\|E_{\boldsymbol{p}}^{\xi}(0)\|^2 \\
\le& \left|\int_0^{\tau}\big(\xi_u, (\eta_u)_t\big)_{\mathcal{T}_h}dt\right| - \int_0^{\tau}\|\xi_u\|^2dt - \int_0^{\tau}\|\xi_{\boldsymbol{q}}\|^2dt + \left|\big(\alpha\eta_u(0), E_u^{\xi}(0)\big)_{\mathcal{T}_h}\right| + \left|\int_0^{\tau}\big(\xi_u, \eta_u\big)_{\mathcal{T}_h}dt\right| \\
&+ \left|\int_0^{\tau}\big(E_{\boldsymbol{p}}^{\eta}, \xi_{\boldsymbol{p}}\big)_{\mathcal{T}_h}dt\right| + \left|\big(E_{\boldsymbol{q}}^{\xi}(0), \xi_{\boldsymbol{q}}(0)\big)_{\mathcal{T}_h}\right| + \left|\int_0^{\tau}\big(\xi_{\boldsymbol{q}}, \eta_{\boldsymbol{q}}\big)_{\mathcal{T}_h}dt\right| + \left|\big(E_{\boldsymbol{q}}^{\eta}(0), \xi_{\boldsymbol{q}}(0)\big)_{\mathcal{T}_h}\right| \\
&+ \left|\sum_{K\in\mathcal{T}_h} A_K^{\beta}\big(E_u^{\eta}(0), \xi_{\boldsymbol{q}}(0)\big)\right| + \int_0^{\tau}\left|\sum_{K\in\mathcal{T}_h} A_K^{\beta}\big(\eta_u, \xi_{\boldsymbol{q}}\big)\right|dt + \int_0^{\tau}\left|\sum_{K\in\mathcal{T}_h} A_K^{\gamma}\big(E_u^{\eta}, \xi_{\boldsymbol{p}}\big)\right|dt \\
&+ \int_0^{\tau}\left|\sum_{K\in\mathcal{T}_h} B_K^{\gamma}\big(\eta_{\boldsymbol{p}}, E_u^{\xi}\big)\right|dt + \int_0^{\tau}\left|\sum_{K\in\mathcal{T}_h} B_K^{\beta}\big((\eta_{\boldsymbol{q}})_t, E_u^{\xi}\big)\right|dt \\
\le& \int_0^{\tau}\|\xi_u\|\|(\eta_u)_t\|dt - \int_0^{\tau}\|\xi_u\|^2dt - \int_0^{\tau}\|\xi_{\boldsymbol{q}}\|^2dt + \|\alpha\eta_u(0)\|\|E_u^{\xi}(0)\| + \int_0^{\tau}\|\xi_u\|\|\eta_u\|dt \\
&+ \int_0^{\tau}\|E_{\boldsymbol{p}}^{\eta}\|\|\xi_{\boldsymbol{p}}\|dt + \big(\|E_{\boldsymbol{q}}^{\xi}(0)\| + \|E_{\boldsymbol{q}}^{\eta}(0)\|\big)\|\xi_{\boldsymbol{q}}(0)\| + \int_0^{\tau}\|\xi_{\boldsymbol{q}}\|\|\eta_{\boldsymbol{q}}\|dt \\
&+ Ch^{k+1}\int_0^{\tau}\|E_u^{\xi}\|dt + Ch^{2k+2} \\
\le& \tau\max_{t\in[0,\tau]}\|\xi_u\|\max_{t\in[0,\tau]}\|(\eta_u)_t\| - \int_0^{\tau}\|\xi_u\|^2dt - \int_0^{\tau}\|\xi_{\boldsymbol{q}}\|^2dt + Ch^{k+1}\|E_u^{\xi}(0)\| + \int_0^{\tau}\|\xi_u\|^2dt \\
&+ \frac{1}{4}\int_0^{\tau}\|\eta_u\|^2dt + Ch^{k+1}\tau\max_{t\in[0,\tau]}\|\xi_{\boldsymbol{p}}\| + Ch^{k+1}\|E_{\boldsymbol{q}}^{\xi}(0)\| + \int_0^{\tau}\|\xi_{\boldsymbol{q}}\|^2dt + \frac{1}{4}\int_0^{\tau}\|\eta_{\boldsymbol{q}}\|^2dt \\
&+ Ch^{k+1}\|\xi_{\boldsymbol{q}}(0)\| + Ch^{k+1}\tau^2\max_{t\in[0,\tau]}\|\xi_u\| + Ch^{2k+2} \\
\le& \tau\max_{t\in[0,\tau]}\|\xi_u\|\max_{t\in[0,\tau]}\|(\eta_u)_t\| + Ch^{k+1}\|E_u^{\xi}(0)\| + Ch^{k+1}\|E_{\boldsymbol{q}}^{\xi}(0)\| + Ch^{2k+2} \\
\le& Ch^{k+1}\tau\big(\max_{t\in[0,\tau]}\|\xi_u\| + \tau\max_{t\in[0,\tau]}\|\xi_u\| + \max_{t\in[0,\tau]}\|\xi_{\boldsymbol{q}}\|\big) + Ch^{2k+2} \\
\le& \frac{1}{4}\max_{t\in[0,\tau]}\|\xi_u\|^2 + Ch^{2k+2}.
\end{aligned}$$

Since it is true for any $\tau \le T$, we can get

$$\frac{1}{2}\|\xi_u(\tau)\|^2 - \frac{1}{2}\|\xi_u(0)\|^2 + \frac{1}{2}\|E_{\boldsymbol{p}}^{\xi}(0)\|^2 \le \frac{1}{4}\max_{t\in[0,\tau]}\|\xi_u\|^2 + Ch^{2k+2},$$

and then

$$\max_{t\in[0,T]}\|\xi_u\|^2 \le Ch^{2k+2},$$

which leads to

$$\max_{t\in[0,T]} \|e_u(t)\| \le Ch^{k+1}.$$

Here the constant C only depends on α, β, γ, T and the solution u, and is independent of the mesh size h. □

4 Time discretization

In this section, we introduce the time discretization to get fully discrete method. In general, the semi-discrete scheme (2.13)-(2.15) can be obtained by the LDG method for spacial discretization. With (2.13) and (2.14) , we can solve $\boldsymbol{p}_h$ and $\boldsymbol{q}_h$ element-by-element in terms of u_h. By eliminating the auxiliary variables $\boldsymbol{p}_h$ and $\boldsymbol{q}_h$ in (2.15), we can get the linear second-order ordinary differential system:

$$M\ddot{\boldsymbol{u}}_h(t) = A\dot{\boldsymbol{u}}_h(t) + B\boldsymbol{u}_h(t), \tag{4.1}$$

where $\boldsymbol{u}_h(t)$ is the solution vector at the time t, M is the mass matrix.

To get a globally high-order accurate scheme in time and space, here we would like to employ the third-order strong stability preserving (SSP) Runge-Kutta (RK) method for the above ordinary differential system. To achieve this, an auxiliary variable $\boldsymbol{v}_h(t)$ is first introduced in (4.1) to get the following first-order system:

$$\begin{aligned} &\dot{\boldsymbol{u}}_h(t) = \boldsymbol{v}_h(t), \\ &M\dot{\boldsymbol{v}}_h(t) = A\boldsymbol{v}_h(t) + B\boldsymbol{u}_h(t). \end{aligned} \tag{4.2}$$

Assume that the time interval $\{t > 0\}$ is discretized as: $t^{n+1} = t^n + \Delta t_n, n = 0, 1, 2, \cdots$, where Δt_n is the time step size at $t = t_n$ and will be determined by the CFL type condition

$$\Delta t_n = \lambda * \min\left\{ \frac{\sqrt{3d}}{2d}\frac{h_{\min}}{\gamma_{\max}}, \frac{h_{\min}^2}{\alpha_{\max}h_{\min}^2 + 4d\beta_{\max}^2} \right\}$$

with d being the dimension, $h = \min_{i,j}\{h_i, h_j\}$ and $\alpha_{\max} = \max_{\boldsymbol{x}\in\Omega}\alpha(\boldsymbol{x})$ and similar definitions to $\beta_{\max}$ and $\gamma_{\max}$. λ is the CFL number. Let u_h^n and v_h^n be the approximations to $u(\cdot, t^n)$ and $v(\cdot, t^n)$, then the third-order SSP RK method is used for the time discretization as follows.

Stage 1:

$$\begin{aligned} \boldsymbol{u}_h^{(1)} &= \boldsymbol{u}_h^n + \Delta t_n \boldsymbol{v}_h^n, \\ M\boldsymbol{v}_h^{(1)} &= M\boldsymbol{v}_h^n + \Delta t_n \left(A\boldsymbol{v}_h^n + B\boldsymbol{u}_h^n\right). \end{aligned} \tag{4.3}$$

Stage 2:

$$\begin{aligned} \boldsymbol{u}_h^{(2)} &= \frac{3}{4}\boldsymbol{u}_h^n + \frac{1}{4}\left(\boldsymbol{u}_h^{(1)} + \Delta t_n \boldsymbol{v}_h^{(1)}\right), \\ M\boldsymbol{v}_h^{(2)} &= \frac{3}{4}M\boldsymbol{v}_h^n + \frac{1}{4}\left(M\boldsymbol{v}_h^{(1)} + \Delta t_n\big(A\boldsymbol{v}_h^{(1)} + B\boldsymbol{u}_h^{(1)}\big)\right). \end{aligned} \tag{4.4}$$

Stage 3:

$$\begin{aligned} \boldsymbol{u}_h^{n+1} &= \frac{1}{3}\boldsymbol{u}_h^n + \frac{2}{3}\left(\boldsymbol{u}_h^{(2)} + \Delta t_n \boldsymbol{v}_h^{(2)}\right), \\ M\boldsymbol{v}_h^{n+1} &= \frac{1}{3}M\boldsymbol{v}_h^n + \frac{2}{3}\left(M\boldsymbol{v}_h^{(2)} + \Delta t_n\big(A\boldsymbol{v}_h^{(2)} + B\boldsymbol{u}_h^{(2)}\big)\right). \end{aligned} \tag{4.5}$$

5 Numerical tests

In this section, we present some numerical examples to demonstrate the accuracy and effectiveness of our LDG schemes. The CFL number λ is taken as $\lambda = 0.25, 0.06, 0.02$ for $k = 1, 2, 3$ respectively.

Example 1. Accuracy test in P^k space for the one-dimensional case.

We consider the one-dimensional diffusive-viscous wave equation with constant coefficients,

$$u_{tt} + 2u_t - u_{txx} - u_{xx} = 0, \quad x \in [0, 1],$$

with initial conditions

$$u(x, 0) = \cos(2\pi x), \quad u_t(x, 0) = a\cos(2\pi x)$$

where $a = \sqrt{4\pi^4 + 1} - 2\pi^2 - 1$. The exact solution is $u(x, t) = \mathrm{e}^{at}\cos(2\pi x)$. We simulate this problem with our LDG method based on the P^k $(k = 1, 2, 3)$ polynomial spaces respectively, and list the numerical errors of u and u_x at the final time $T = 0.5$ in the Tables 5.1-5.3. We can observe clearly that the optimal convergence rate ($(k+1)$-th order) can be achieved in both u and u_x as expected.

Table 5.1: The numerical errors and orders with uniform meshes and P^1 space.

N	Error of u					
	L^1 error	Order	L^2 error	Order	L^∞ error	Order
10	7.743E-03		1.042E-02		3.862E-02	
20	1.916E-03	2.015	2.608E-03	1.993	9.897E-03	1.964
40	4.777E-04	2.004	6.522E-04	1.998	2.489E-03	1.991
80	1.194E-04	2.001	1.631E-04	2.000	6.233E-04	1.998
160	2.983E-05	2.000	4.076E-05	2.000	1.559E-04	1.999

N	Error of u_x					
	L^1 error	Order	L^2 error	Order	L^∞ error	Order
10	4.842E-02		6.512E-02		2.484E-01	
20	1.202E-02	2.010	1.636E-02	1.993	6.178E-02	2.007
40	3.001E-03	2.002	4.096E-03	1.998	1.562E-02	1.984
80	7.499E-04	2.001	1.024E-03	2.000	3.915E-03	1.996
160	1.874E-04	2.000	2.561E-04	2.000	9.794E-04	1.999

Table 5.2: The numerical errors and orders with uniform meshes and P^2 space.

N	Error of u					
	L^1 error	Order	L^2 error	Order	L^∞ error	Order
10	3.826E-04		5.228E-04		2.444E-03	
20	4.742E-05	3.012	6.562E-05	2.994	3.055E-04	3.000
40	5.912E-06	3.004	8.211E-06	2.999	3.848E-05	2.989
80	7.385E-07	3.001	1.027E-06	3.000	4.818E-06	2.997
160	9.230E-08	3.000	1.283E-07	3.000	6.026E-07	2.999

N	Error of u_x					
	L^1 error	Order	L^2 error	Order	L^∞ error	Order
10	2.321E-03		3.285E-03		1.465E-02	
20	2.980E-04	2.961	4.123E-04	2.994	1.912E-03	2.938
40	3.715E-05	3.004	5.159E-05	2.999	2.415E-04	2.985
80	4.640E-06	3.001	6.451E-06	3.000	3.027E-05	2.996
160	5.799E-07	3.000	8.064E-07	3.000	3.786E-06	2.999

Table 5.3: The numerical errors and orders with uniform meshes and P^3 space.

N	Error of u					
	L^1 error	Order	L^2 error	Order	L^∞ error	Order
10	1.435E-05		2.021E-05		1.038E-04	
20	9.220E-07	3.961	1.268E-06	3.995	6.700E-06	3.954
40	5.751E-08	4.003	7.930E-08	3.999	4.221E-07	3.988
80	3.593E-09	4.000	4.958E-09	4.000	2.653E-08	3.992

N	Error of u_x					
	L^1 error	Order	L^2 error	Order	L^∞ error	Order
10	9.350E-05		1.270E-04		6.770E-04	
20	5.794E-06	4.012	7.965E-06	3.995	4.197E-05	4.012
40	3.613E-07	4.003	4.983E-07	3.999	2.650E-06	3.985
80	2.258E-08	4.000	3.115E-08	4.000	1.666E-07	3.991

Example 2. Accuracy test in Q^k space for the two-dimensional case.

We consider the one-dimensional diffusive-viscous wave equation with constant coefficients,

$$u_{tt} + 2u_t - \partial_t(\Delta u) - \Delta u = 0, \quad (x, y) \in [0, 1]^2,$$

with initial conditions

$$u(x, y, 0) = \cos(2\pi x), \quad u_t(x, y, 0) = a\cos(2\pi x)$$

where $a = \sqrt{16\pi^4 + 1} - 4\pi^2 - 1$. This problem has the exact solution $u(x, y, t) = \mathrm{e}^{at}\cos(2\pi x)\cos(2\pi y)$. We implement the LDG method on Cartesian meshes with Q^k $(k = 1, 2)$ polynomial spaces until the final time $T = 0.5$. The numerical errors of u, u_x and u_y, and corresponding orders are shown in the Tables 5.4-5.5. For Q^1 and Q^2, the optimal orders of accuracy can be obtained for u, u_x, u_y.

Table 5.4: The numerical errors and orders with uniform meshes and Q^1 space.

$N \times M$	Error of u					
	L^1 error	Order	L^2 error	Order	L^∞ error	Order
10×10	6.992E-03		1.028E-02		7.851E-02	
20×20	1.753E-03	1.995	2.587E-03	1.990	1.979E-02	1.988
40×40	4.381E-04	2.001	6.478E-04	1.998	4.955E-03	1.998
80×80	1.095E-04	2.000	1.620E-04	1.999	1.239E-03	1.999

$N \times M$	Error of u_x					
	L^1 error	Order	L^2 error	Order	L^∞ error	Order
10×10	4.418E-02		6.414E-02		4.859E-01	
20×20	1.103E-02	2.001	1.623E-02	1.983	1.235E-01	1.976
40×40	2.754E-03	2.002	4.068E-03	1.996	3.108E-02	1.991
80×80	6.881E-04	2.001	1.018E-03	1.999	7.783E-03	1.998

$N \times M$	Error of u_y					
	L^1 error	Order	L^2 error	Order	L^∞ error	Order
10×10	4.418E-02		6.414E-02		4.859E-01	
20×20	1.103E-02	2.001	1.623E-02	1.983	1.235E-01	1.976
40×40	2.754E-03	2.002	4.068E-03	1.996	3.108E-02	1.991
80×80	6.881E-04	2.001	1.018E-03	1.999	7.783E-03	1.998

Table 5.5: The numerical errors and orders with uniform meshes and Q^2 space.

$N \times M$	Error of u					
	L^1 error	Order	L^2 error	Order	L^∞ error	Order
5×5	3.044E-03		3.988E-03		2.763E-02	
10×10	3.945E-04	2.948	5.163E-04	2.949	3.017E-03	3.195
20×20	4.966E-05	2.990	6.511E-05	2.987	3.393E-04	3.153
40×40	6.217E-06	2.998	8.156E-06	2.997	4.060E-05	3.063

$N \times M$	Error of u_x					
	L^1 error	Order	L^2 error	Order	L^∞ error	Order
5×5	1.936E-02		2.540E-02		1.881E-01	
10×10	2.483E-03	2.963	3.255E-03	2.964	1.905E-02	3.304
20×20	3.122E-04	2.991	4.094E-04	2.991	2.197E-03	3.116
40×40	3.907E-05	2.998	5.126E-05	2.998	2.587E-04	3.086

$N \times M$	Error of u_y					
	L^1 error	Order	L^2 error	Order	L^∞ error	Order
5×5	1.936E-02		2.540E-02		1.881E-01	
10×10	2.483E-03	2.963	3.255E-03	2.964	1.905E-02	3.304
20×20	3.122E-04	2.991	4.094E-04	2.991	2.197E-03	3.116
40×40	3.907E-05	2.998	5.126E-05	2.998	2.587E-04	3.086

Example 3. Wave propagation within homogeneous medium.

We consider the 2D homogeneous medium model with the size of $[0,1] \times [0,1]$. In the diffusive-viscous wave equation (2.1), we set the parameters as $\alpha = 0, \beta = 0.1$ and $\gamma = 0.4$. A Ricker wavelet with dominant frequency of 15Hz located at $(x_0, y_0) = (0.5, 0.5)$ is used to generate the vibration. To achieve that, we can describe the source function as follows

$$f(x,y,t) = g(x,y)h(t),\ \ g(x,y) = \mathrm{e}^{-100[(x-x_0)^2+(y-y_0)^2]},\ \ h(t) = \big[1-2(\pi f_0(t-0.1))^2\big]\mathrm{e}^{-(\pi f_0(t-0.1))^2}, \tag{5.1}$$

where f_0 is the dominant frequency, i.e, $f_0 = 15$.

We use the LDG method with Q^2 space on uniform mesh and the third-order SSP Runge-Kutta method to simulate this model. The zero boundary conditions are imposed. Figure 5.1 shows the time evolution of the diffusive-viscous wave. It is clear to observe that the wave propagates outward isotropically from the source center (x_0, y_0). We further compare the cross sections of the numerical solutions at the line $y = x$ for $T = 0.05, 0.3, 0.5$ in Figure 5.2 to verify the convergence of the numerical solutions. It can be seen that the one-dimensional profiles match very well.

(a) $T = 0.05$ (b) $T = 0.3$ (c) $T = 0.5$

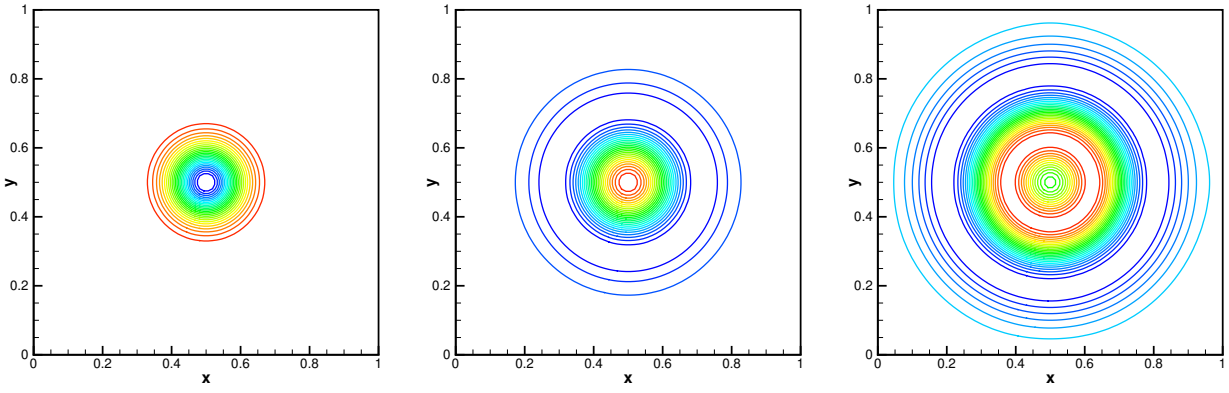

Figure 5.1: Contours of the numerical approximations at time $T = 0.05, 0.3, 0.5$. The grid is uniform with 80×80 cells.

(a) $T = 0.05$ (b) $T = 0.3$ (c) $T = 0.5$

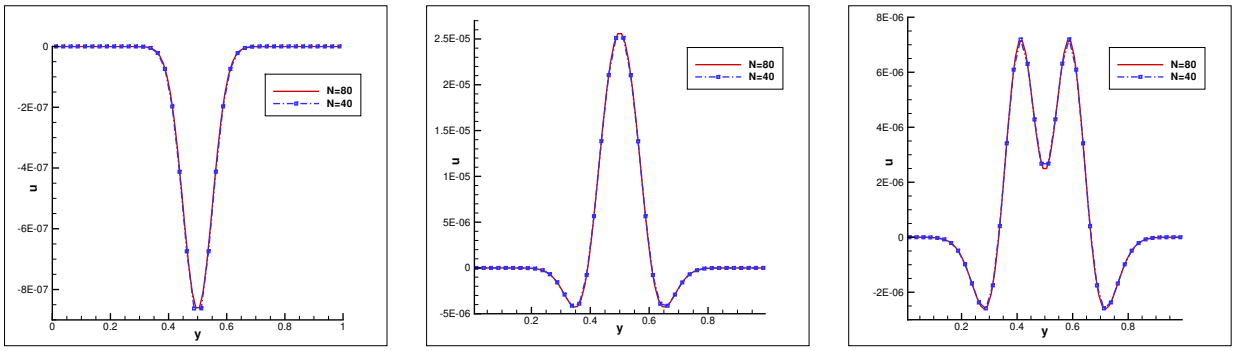

Figure 5.2: Comparison of the cross sections of the numerical solutions at $y = x$, at $T = 0.05, 0.3, 0.5$. The red solid lines are for 80×80 cells, and the blue dash-dotted lines with the symbol are for 40×40 cells.

Example 4. Wave propagation within heterogeneous media.

We consider the 2D diffusive-viscous wave equation (2.1) with discontinuous coefficients. The computational domain is $[0, 1.5] \times [0, 1.5]$. The coefficients are defined as

$$(\alpha, \beta, \gamma) = \begin{cases} (1, 0.1, 0.5), & \text{if } \ y \leq 0.8, \\ (2.5, 0.2, 0.2), & \text{if } \ y > 0.8. \end{cases}$$

The source function is described as that in (5.1) with $(x_0, y_0) = (0.7, 0.7)$ and $f_0 = 15$.

We simulate this model with the LDG method by using Q^2 space on uniform mesh and the third-order SSP Runge-Kutta method. The zero boundary conditions are employed. Figures 5.3 and 5.4 show the time evolution of the diffusive-viscous wave propagation. We can see that initially the wave propagates isotropically until it reaches the interface of different media (around $T = 0.15$ to 0.25), and at a later time the wave fronts propagate at different speeds in these two media. Figure 5.4 illustrates the cross sections at the line $y = 1.0$, and we can observe that these one-dimensional profiles match very well for different mesh sizes, which verifies the numerical convergence of our method.

(a) $T = 0.08$ (b) $T = 0.15$ (c) $T = 0.25$

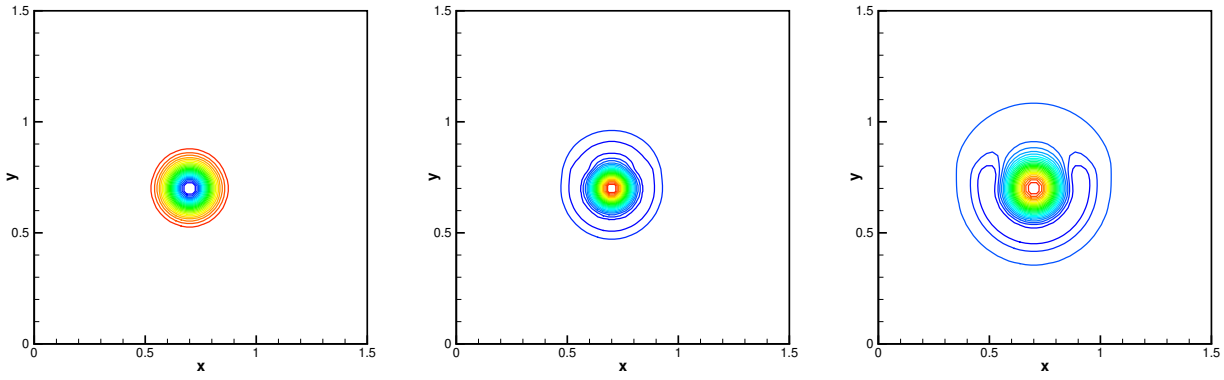

(d) $T = 0.3$ (e) $T = 0.4$ (f) $T = 0.5$

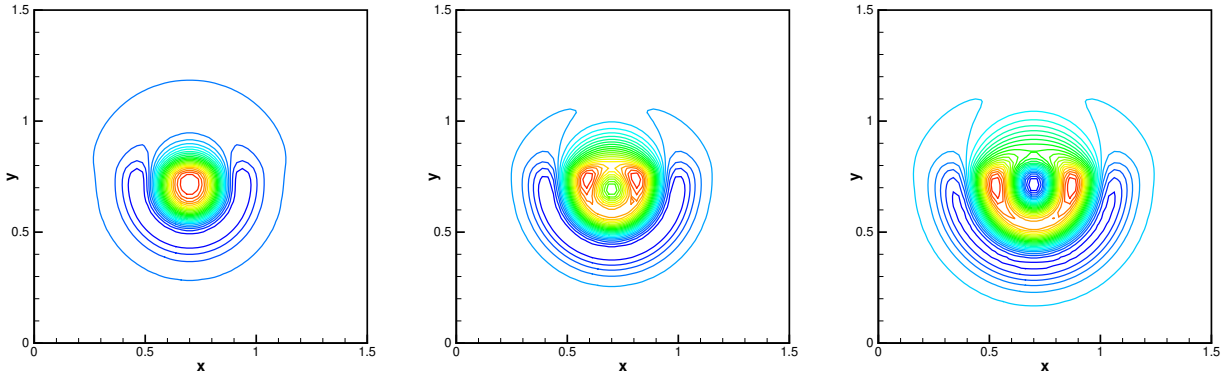

Figure 5.3: Contours of the numerical solutions at time $T = 0.08, 0.15, 0.25, 0.3, 0.4, 0.5$. The grid is uniform with 60×60 cells.

(a) $T = 0.08$ (b) $T = 0.15$ (c) $T = 0.25$

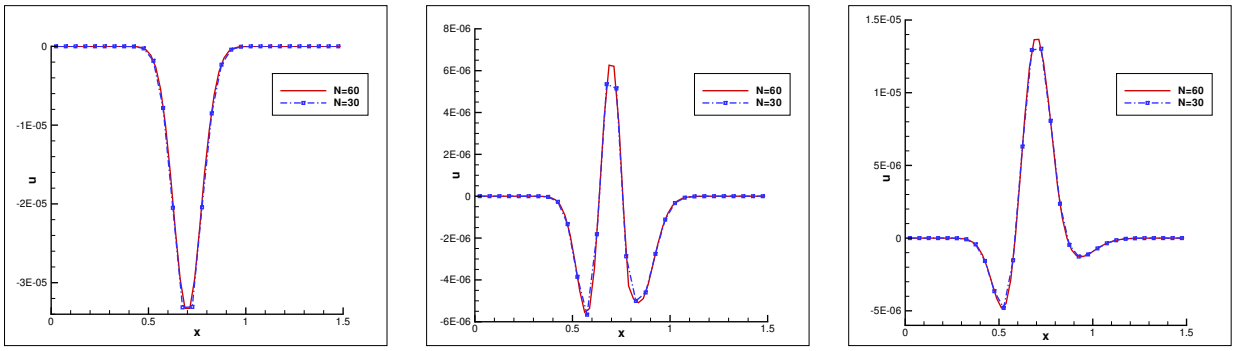

(d) $T = 0.3$ (e) $T = 0.4$ (f) $T = 0.5$

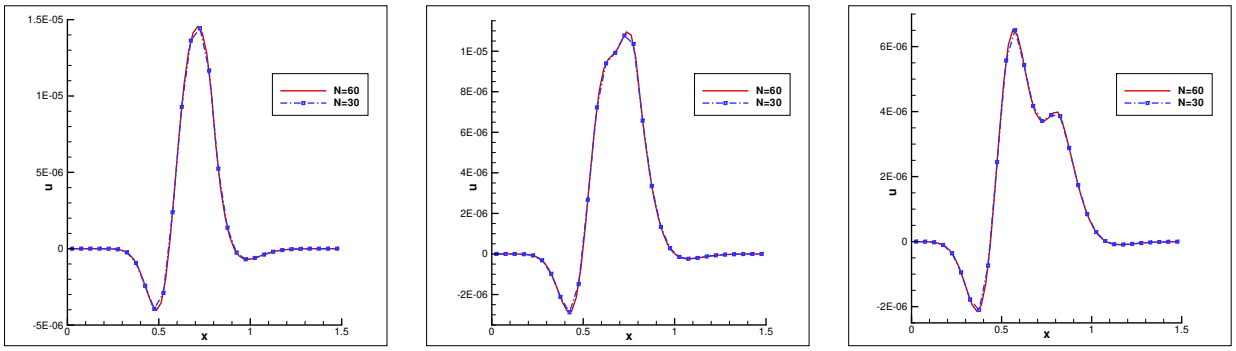

Figure 5.4: Comparison of the cross sections of the numerical solutions at $y = 1.0$, at $T = 0.08, 0.15, 0.25, 0.3, 0.4, , 0.5$. The red solid lines are for 60×60 cells, and the blue dash-dotted lines with the symbol are for 30×30 cells.

6 Conclusions

In this paper, we have developed an LDG method for multi-dimensional diffusive-viscous wave problems which allow discontinuous media. The numerical fluxes have been chosen carefully to make the method stable and guarantee the continuity of the flux. For the proposed LDG method, we have proved the optimal error estimates in both the energy norm and the L^2 norm. The theoretical results are confirmed by some numerical examples. From a more practical point of view, to simulate the seismic wave propagation in a finite domain, absorbing boundary conditions are often used to avoid the artificial reflection phenomenon. Therefore we would like to develop the LDG method for the diffusive-viscous wave equation with absorbing boundary conditions as our future work.

References

[1] M.A. Biot, Theory of propagation of elastic waves in a fluid-saturated porous solid. I. Low frequency range, *J. Acoust. Soc. Amer.*, 28 (1956) 168-178.

[2] M.A. Biot, Theory of propagation of elastic waves in a fluid-saturated porous solid. II. Higher frequency range, *J. Acoust. Soc. Amer.*, 28 (1956) 179-191.

[3] M.A. Biot, Generalized theory of acoustic propagation in porous dissipative media, *J. Acoust. Soc. Amer.*, 34 (1962) 1254-1264.

[4] X.H. Chen, Z.H. He, X.G. Pei,et al, Numerical simulation of frequency-dependent seismic response and gas reservoir delineation in turbidites: A case study from China, *J. Appl. Geophy.*, 94 (2013) 22-30.

[5] Y. Cheng, C.-W. Shu, Superconvergence of discontinuous Galerkin and local discontinuous Galerkin schemes for linear hyperbolic and convection diffusion equations in one space dimension, *SIAM J. Numer. Anal.*, 47 (2010) 4044-4072.

[6] C.-S. Chou, C.-W. Shu, Y. Xing, Optimal energy conserving local discontinuous Galerkin methods for second-order wave equation in hetergeneous media, *J. Comput. Phys.*, 272 (2014) 88-107.

[7] B. Cockburn, S. Hou, C.-W. Shu, The Runge-Kutta local projection discontinuous Galerkin finite element method for conservation laws IV: the multi-dimensional case, *Math. Comput.*, 54 (1990) 545-581.

[8] B. Cockburn, S.-Y. Lin, C.-W. Shu, TVB Runge-Kutta local projection discontinuous Galerkin finite element method for conservation laws III: one dimensional systems, *J. Comput. Phys.*, 84 (1989) 90-113.

[9] B. Cockburn, C.-W. Shu, TVB Runge-Kutta local projection discontinuous Galerkin finite element method for conservation laws II: general framework, *Math. Comput.*, 52 (1989) 411-435.

[10] B. Cockburn, C.-W.Shu, The local discontinuous Galerkin method for time-dependent convection-diffusion systems, *SIAM J. Numer. Anal.*, 35 (1998) 2440-2463.

[11] B. Cockburn, C.-W. Shu, The Runge-Kutta discontinuous Galerkin method for conservation laws V: multidimensional systems, *J. Comput. Phys.*, 141 (1998) 199-224.

[12] B. Cockburn, C.-W. Shu, Runge-Kutta discontinuous Galerkin methods for convection-dominated problems, *J. Sci. Comput.*, 16 (2001) 173-261.

[13] B. Dong, C.-W. Shu, Analysis of a local discontinuous Galerkin method for linear time-dependent fourth-order problems, *SIAM J. Numer. Anal.*, 47 (2009) 3240-3268.

[14] J. Dvorkin, G. Mavko, A. Nur, Squirt flow in fully saturated rocks, *Geophysics*, 60 (1995) 97-107.

[15] G.M. Goloshubin, A.V. Bakulin, Seismic reflectivity of a thin porous fluid-saturated layer versus frequency, *SEG Technical Program Expanded Abstracts*, (1998) 976-979.

[16] W. Han, J. Gao, Y. Zhang, W. Xu, Well-posedness of the diffusive-viscous wave equation arising in geophysics, *J. Math. Anal. Appl.*, 486 (2020) 123914.

[17] Z.H. He, X.J. Xiong, L.E. Bian, Numerical simulation of seismic low-frequency shadows and its application, *Appl. Geophys.*, 45 (2008) 301-306.

[18] C. Hufford, Y. Xing, Superconvergence of the local discontinuous Galerkin method for the linearized Korteweg-deVries equation, *J. Comput. Appl. Math.*, 255 (2014) 441-455.

[19] V.A. Korneev, G.M. Goloshubin, T.M. Daley, D.B. Silin, Seismic low-frequency effects in monitoring fluid-saturated reservoirs, *Geophysics*, 69 (2004) 522-532.

[20] X. Meng, C.-W. Shu, B. Wu, Superconvergence of the local discontinuous Galerkin method for linear fourth order time dependent problems in one space dimension, *IMA J. Numer. Anal.*, 32 (2012) 1294-1328.

[21] V. Mensah, A. Hidalgo, R.M. Ferro, Numerical modelling of the propagation of diffusive-viscous waves in a fluid-saturated reservoir using finite volume method, *Geophys. J. Int.*, 218 (2019) 33-44.

[22] B. Quintal, S.M. Schmalholz, Y.Y. Podladchikov, J.M. Carcione, Seismic low-frequency anomalies in multiple reflections from thinly layered poroelastic reservoirs, *SEG Technical Program Expanded Abstracts*, (2007) 1690-1695.

[23] Y. Xing, C.-S. Chou, C.-W. Shu, Energy conserving local discontinuous Galerkin methods for wave propagation problems, *Inverse Prol. Imaging*, 7 (2013) 967-986.

[24] J. Yan, C.-W. Shu, A local discontinuous Galerkin method for KdV type equations, *SIAM J. Numer. Anal.*, 40(2) (2002) 769-791.

[25] H.X. Zhao, J.H. Gao, Z.X. Chen, Stability and numerical dispersion analysis of finite difference method for the diffusive-viscous wave equation, *Int. J. Numer. Anal. Model. Ser. B*, 5 (2014) 66-78.

[26] H.X. Zhao, J.H. Gao, J. Zhao, Modeling the propagation of diffusive-viscous waves using flux-corrected transport-finite-difference method, *IEEE J. Sel. Top. Appl. Earth Obs. Remote Sens.*, 7 (2014) 838-844.